SYNTHESIS AND CHARACTERISATION OF BULK AND ALKALINE EARTH METAL DOPED VANADYL PYROPHOSPHATE CATALYSTS

By

THANG LEE YIEN

A dissertation submitted to the Department of Chemical Engineering,
Faculty of Engineering and Science,
Universiti Tunku Abdul Rahman,
in partial fulfillment of the requirements for the degree of
Master of Science
November 2013

ABSTRACT

SYNTHESIS AND CHARACTERISATION OF BULK AND ALKALINE EARTH METAL DOPED VANADYL PYROPHOSPHATE CATALYSTS

THANG LEE YIEN

Vanadium phosphate catalysts were prepared via vanadyl hydrogen phosphate sesquihydrate route. The synthesized VPS precursors were doped with alkaline earth metals, e.g. Mg, Ca, Sr and Ba and activated at 733 K in a reaction flow of 1% O_2/N_2 to generate the active vanadyl pyrophosphate, $(VO)_2P_2O_7$ catalysts. The effect of activation duration for undoped and Ba-doped VPS catalysts was examined. The optimum activation duration was selected and proceeded with the study of the effect on Mg, Ca and Sr doped VPS catalysts. The characterisation of the VPS catalysts including XRD, BET, SEM, EDX, TPD of O_2, TPR in H_2, ICP-OES and redox titration. The catalytic performances of these catalysts were determined by using a fixed-bed microreactor. XRD patterns for the undoped and Ba-doped VPS catalysts comprised of well-crystallised $(VO)_2P_2O_7$ phase. BET analyses showed that the specific surface area of the undoped and Ba-doped VPS catalysts were inversely proportional to the activation duration. The amount of V^{4+} was inversely proportional to the activation duration. This is in agreement with the specific surface area results, which showed that VPS catalysts with higher amount of V^{4+} gave higher specific surface area. SEM analysis revealed that undoped and Ba-doped VPS catalysts consisted of plate-like crystals with

folded edges. The amount of oxygen atom removed from the undoped and Ba-doped VPS catalysts increased with activation duration indicated an increased reactivity and mobility of lattice oxygen. Catalytic characterisation showed that *n*-butane conversion decreased as activation duration increased. However, the selectivity to maleic anhydride was not markedly affected by activation duration. The optimum activation duration obtained was 6 hours. The Mg, Ca and Sr doped VPS catalysts comprised of well-crystallized $(VO)_2P_2O_7$ phase. There was a trend of increasing specific surface area with increasing amount of V^{4+} when doped from Mg to Sr. The morphology of the Mg, Ca and Sr doped VPS catalysts consisted of plate-like crystals with folded edges. The addition of dopant with Mg, Ca and Sr induced greater amount of oxygen species removed from the VPS catalysts, which had shown an increased reactivity and mobility of lattice oxygen. Catalytic performance revealed that VPS catalyst doped with Sr had the highest *n*-butane conversion and selectivity to maleic anhydride compared to Mg and Ca.

ACKNOWLEDGEMENT

I would like to take this opportunity to thank Univesiti Tunku Abdul Rahman (UTAR) for providing the ground education and research. I would like to express my greatest gratitude to Dr. Leong Loong Kong who not only serves as a supervisor but also as a role model for me through his diligence, patience, wisdom and tenacity despite failures and hardships.

I would like to take this opportunity to thank seniors, team mates and friend for their advices and supports throughout the project. I would like to express my deepest appreciation to my family for their continuous support and encouragement.

APPROVAL SHEET

This dissertation entitled "**SYNTHESIS AND CHARACTERISATION OF BULK AND ALKALINE EARTH METAL DOPED VANADYL PYROPHOSPHATE CATALYSTS"** was prepared by THANG LEE YIEN and submitted as partial fulfillment of the requirements for the degree of Master of Science at Universiti Tunku Abdul Rahman.

Approved by:

_____

(Asst. Prof. Dr. Leong Loong Kong) Date:……..
Supervisor
Department of Chemical Engineering
Faculty of Engineering and Science
Universiti Tunku Abdul Rahman

FACULTY OF ENGINEERING AND SCIENCE

UNIVERSITI TUNKU ABDUL RAHMAN

Date: _____

SUBMISSION OF DISSERTATION

It is hereby certified that THANG LEE YIEN (ID No: 09UEM09097) has completed this dissertation entitled "**SYNTHESIS AND CHARACTERISATION OF BULK AND ALKALINE EARTH METAL DOPED VANADYL PYROPHOSPHATE CATALYSTS**" under the supervision of Dr. Leong Loong Kong (Supervisor) from the Department of Chemical Engineering, Faculty of Engineering and Science.

I understand that University will upload softcopy of my thesis in pdf format into UTAR Institutional Repository, which may be made accessible to UTAR community and public.

Yours truly,

_____

(*Thang Lee Yien*)

DECLARATION

I THANG LEE YIEN hereby declare that the dissertation is based on my original work except for quotations and citations which have been duly acknowledged. I also declare that it has not been previously or concurrently submitted for any other degree at UTAR or other institutions.

_____

(THANG LEE YIEN)

Date _____

TABLE OF CONTENTS

LIST OF TABLES

LIST OF FIGURES

LIST OF ABBREVIATIONS

VPO	**Vanadium Phosphorus Oxide**
VPS	**Vanadium Phosphate Sesquihydrate**
MA	**Maleic Anhydride**
VPP	**Vanadyl Pyrophosphate**
CFB	**Circulating-Fluid Bed**
LPG	**Liquefied Petroleum Gas**
WP	**World Petrochemical**
XRD	**X-Ray Diffraction**
BET	**Brunauer, Emmett and Teller**
ICP-OES	**Inductive Coupled Plasma-Optical Emission Spectroscopy (ICP- OES)**
SEM	**Scanning Electron Microscope**
EDX	**Energy Dispersive X-Ray**
TPDRO	**Temperature-Programmed Desorption, Reduction and Oxidation**
TPD	**Temperature-Programmed Desorption**
TPR	**Temperature Programmed Reduction**
TON	**Turnover number**
TCD	**Thermal Conductivity Detector**
P/V	**Phosphorus to Vanadium ratio**
FWHM	**Full-width at half maximum**
t	**Crystallite size**
ppm	**Parts per million**
JCPDS	**Joint Committee on Powder Diffraction Standards**

CHAPTER 1.0

INTRODUCTION

1.1 Catalysis

Catalysts are the workhorses of chemical transformation in industries that offer an alternative and energetically favorable mechanism to the non-catalytic reaction, enabling the processes to be carried out under industrially feasible temperature and pressure (Chorkendorff and Niemantsverdriet, 2003). For instance, catalyst is the indispensable part of transportation fuel production in one of the approximately 440 oil refineries all over the world.

Catalysis can be classified into two major groups: homogeneous catalysis and heterogeneous catalysis. Homogeneous catalysis occurs in a uniform gas or liquid phase while heterogeneous catalysis takes place between several phases i.e. generally the catalyst is a solid and the reactants are liquid or gases (Hagen, 2006). Vanadium phosphate catalyst is one of the most well studied heterogeneous catalysts capable of selective oxidation of alkanes (Sartoni et al., 2004).

A catalyst used for industrial processes depends on three properties: activity, selectivity and stability (Hagen, 2006). Activity is a measure of how fast one or more reactions proceed in the presence of catalyst. Kinetically, activity is a measure of reaction rates in the temperature and concentration ranges. Another measure of catalyst activity is the turnover number (TON).

TON specifies the maximum use that can be made of a catalyst for a special reaction under defined conditions. In homogeneous catalysis, the catalyst molecules are well-defined and therefore the TON can be determined directly. However, this is difficult in heterogeneous catalysis since the catalyst does not have the uniform structure but the activity depends on the size of the catalyst surface. The selectivity of a reaction is the fraction of the starting material that is converted to the desired product. Catalyst stability is a measurement of its lifetime in industrial reactors and influenced by numerous factors including decomposition, coking and poisoning.

1.2 Selective Oxidation

The best-known selective oxidation processes applied large-scale in industries including: oxidation of ethylene to ethylene oxide, oxidation of propene to acrolein and ammoxidation to acrylonitrile, oxidation of *n*-butane, butenes or benzene to maleic anhydride, oxidation of *o*-xylene to phthalic anhydride (Hagen, 2006).

Selective oxidation of catalysts is important in functionalization of alkenes and aromatics due to the ease and economy with which they can be obtained from petroleum (Datta et al., 2002). Nowadays, selective oxidation is used in functionalization of alkanes directly since it is more economical and raw materials are readily available (Datta et al., 2002).

Selective oxidation reactions on reducible metal oxides are generally believed to follow the Mars and van Krevelen mechanism (Coulston et al., 1996). The catalytic center is an assembly of a Lewis acid site, a Lewis basic site, and a metal atom that undergoes variation in its oxidation state through the catalytic cycle (Corma and Garcia, 2002). The Mars and Krevelen mechanism consists of a series of elementary steps that include: (i) activation of substrate on a metallic cation; (ii) insertion of oxygen from lattice oxygen; and (iii) a redox process at the metallic site and the transfer of one or several electrons. In the first step, metallic cations act as Lewis acid sites, and the basic sites are surface $O^{=}$ or OH^{-} species. The substrate undergoes hydrogen abstraction, oxygen insertion, and electron transfer. Thus, the active sites require a spatial organization at atomic level and the cooperation of distinctive atoms. The oxidation of *n*-butane to maleic anhydride is believed to occur via this mechanism (Corma and Garcia, 2002).

The selective oxidation of hydrocarbons are very challenging because: (i) thermodynamics favours the total oxidation of the hydrocarbon to carbon dioxide and water and therefore the selective oxidation product has to be obtained by kinetic control of product; (ii) all oxidation reactions are strongly exothermic and efficient heat removal has to be done to control the temperature and prevent over-oxidation; (iii) the C-H bonds in the initial reactant are usually stronger than those in the intermediate products, which make the intermediates prone to rapid further oxidation; (iv) the hydrocarbon-oxygen mixture can react along several different pathways and catalyst must control

the relative rates accelerating the steps leading to the desired product and hindering those which gives unwanted products (Dutta, 2005).

The key step in selective oxidation therefore is to stop the oxidation at the desired compound through kinetic control. This can be done by desiring the nature of active sites of the catalyst such that it is able to control the relative rates of different reaction pathways- accelerating the steps leading to the desired product and hindering those which give unwanted products (Dutta, 2005).

The control of selectivity by nature of active sites is the apparent paradox of catalytic chemistry that higher yield and selectivity are obtained in the oxidation of *n*-butane than in the oxidation of butenes using a vanadyl pyrophosphate catalyst. This is because when the olefin is directly as the feedstock, due to its high nucleophilicity of the olefin may easily interact with different sites other than those able to transform it directly to the final anhydrides. In contrast, butane absorbs on sites responsible for its dehydrogenation which is the first step followed by rapid oxidation to the anhydride (Dutta, 2005).

In any industrial process, it is endeavoured to achieve highest possible conversion with close to 100% selectivity of the desired product. In reality, it is difficult to attain both simultaneously, as the conversion and selectivity do not go hand in hand and at times they are related inversely (Chilukuri et al., 2005).

Vanadium is among the most active transition metals that capable to effectual alkane oxydehydrogenation, oxygenations, and alkylaromatic oxidations (Corma and Garcia, 2002). For the selective oxidation of *n*-butane to maleic anhydride by vanadyl pyrophosphate, the process is suppose to occur specifically on (100) face of crystal, which is supported by the spatial distribution of atoms in the catalyst exposed to the C-C and C-H bonds of *n*-butane (Corma and Garcia, 2002). The catalyst requires the simultaneous presence of surface redox and acid sites and the acidity as well in order to control the further kinetic steps of *n*-butane oxidation (Corma and Garcia, 2002).

The oxidation of *n*-butane to maleic anhydride involves a one-step reaction:

$$C_4H_{10} + 7/2\ O_2 \rightarrow C_4H_2O_3 + 4H_2O$$

The oxidation of *n*-butane to maleic anhydride is the most successful process since it activates the poorly reactive butane and abstracting eight protons without cleaving a C-C bond. The three oxygen atoms are attached without forming any carbon oxides as the maleic anhydride is kinetically stable against further oxidation at the remaining protons. The locations of further attack are strongly bound to the cyclic carbon skeleton. The reaction occurs in many intermediate steps that are all stabilized against oxidative oxidative attack due to the chemisorptions at an active site that has to become progressively less active during the whole transformation (Corma and Garcia, 2002).

Vanadium phosphorus oxide (VPO) catalysts are commercially applied in industry for the selective oxidation of *n*-butane to maleic anhydride (MA) since its discovery by Bergmann and Frisch, followed by Monsanto in 1974 (Goh et al., 2008). Previously, Maleic anhydride was produced by using benzene as a feedstock but replaced by *n*-butane due to higher price of benzene and restrictions imposed on using benzene from a pollution point of view (Bej and Rao, 1992). In fact, the study of oxidation of butenes to maleic anhydride was started in the early 1970s since butenes and butadiene were inexpensive and available worldwide and only later it was realized that the more viable route involved the use of *n*-butane as raw material (Cavani and Trifirò, 1994).

The conversion of *n*-butane to MA has been the subject of extended research due to economic importance of MA as chemical intermediates and fundamental reason that this reaction is a very complex reaction since it involves a 14-electron oxidation with 8-H abstractions, 3-O insertions, and subsequent electron transfers (Govender et al., 2004). Conversation of *n*-butane to maleic anhydride is the only heterogeneously catalyzed, alkane-selective oxidation that applied commercially (Coulston et al., 1996).

The selective oxidation of *n*-butane to maleic anhydride, catalysed by vanadyl pyrophosphate (VPP), $(VO)_2P_2O_7$ is consolidated at an industrial level since many years with different technologies, i.e., fixed-bed, fluidized-bed and circulating-fluid bed (CFB) reactors (Ballarini et al., 2005). Each technology present some disadvantages: the fixed-bed reactor is limited to low butane concentration, which is less than 2%; the fluidized-bed and the CFB allow high

butane concentration operation but the catalyst attrition can be a major drawback (Cruz-López, 2005).

The modern industrialized world would be impossible without catalysts. However, the developments in catalysis during the last 20 years have been mandated mainly by considerations related to the abatement and prevention of pollution, conservation of raw materials and energy, use of alternate materials and production of more efficient drugs (Sivasanker, 2002). The selective oxidation of organic compounds directly to alcohols, ketones and acids is not easy as the intermediates are more easily oxidized to carbon oxides. The yields of the desired products are low and not environmentally clean. Thus, the cleaner processes based on the use of solid, recoverable catalysts and oxygen or peroxides have been developed.

1.3 The Importance of Catalysis

Most products produced in the chemical and petroleum industry utilize catalysts to enhance the rate of reaction and selectivity to desired products. Heterogeneous catalysts are used on a large scale in the following areas: (i) production of organic and inorganic chemicals; (ii) crude oil refining and petrochemistry; (iii) environmental protection; (iv) energy conversion processes (Hagen, 2006).

Heterogeneous catalysts are used on a large scale in the production of organic chemicals (Hagen, 2006). For instance, bauxite, Al_2O_3 is used as a

catalyst in Claus process to produce sulphur at 300-350 °C, In crude oil processing, catalytic processes are used to produce products such as gasoline, diesel, kerosene, heating oil, aromatic compounds, and liquefied petroleum gas (LPG) in high yield and good quality. Some of the most important processes in refinery technology including: hydrogenation of benzene to cyclohexane using reney Ni as a catalyst; oxidation of ethylene and ethylene oxide with Ag support as a catalyst; and ammoxidation of propene to acrylonitrile using Bi molybdate as a catalyst.

Heterogeneous catalysts have numerous applications in the catalytic afterburning of impurities or odoriferous components in industrial off-gases. Catalytic afterburning can solve various emission problems without generating secondary pollutants. As early as the 1940s, supported Pt/Al_2O_3 catalysts were used for the catalytic purification of off-gases by oxidation. Nowadays, catalysts such as Pt, Pd, Rh, washcoat Al_2O_3, ceramic monoliths and rare earth oxide promoters are applied in automobile exhaust control (Hagen, 2006).

1.4 Problem Statements

The selective oxidation process still offers interesting development possibilities since the economic operation of industrial oxidation process requires a selectivity of at least 60%. The selectivity has improved to over 90% in some cases and thus the space-time yields of the process could be improved and a better use made of raw materials (Hagen, 2006).

Nowadays, the best yield of *n*-butane to MA in industrial process is close to 60%, corresponding to 75% *n*-butane conversion and 80% MA selectivity (Cruz-López et al., 2005).

1.5 Research Objectives

The objectives of this research are:

i. To synthesize the bulk and alkaline earth metals doped vanadium phosphorus oxide catalysts via vanadyl hydrogen phosphate sesquihydrate precursor route.
ii. To study the physical, chemical, reactivity and catalytic characteristics of the synthesised VPS catalysts.
iii. To obtain the optimum activation duration for both bulk and Ba-doped VPS catalysts activated in 1% O_2/N_2 prepared via vanadyl hydrogen phosphate sesquihydrate route.
iv. To investigate the effect of Mg, Ca and Sr-doped VPS catalysts activated in 1% O_2/N_2 prepared via vanadyl hydrogen phosphate sesquihydrate route.

Chapter 2

Literature Review

2.1 Maleic Anhydride

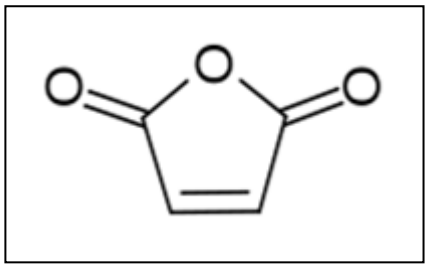

Figure 2.1: Structure of maleic anhydride (MA)

Maleic anhydride (MA), or chemically known as the furan-2,5-dione, is an organic compound with the chemical formula of $C_2H_2(CO)_2O$. MA has significant commercial interest due to its various industrial usages. MA is used in the manufacturing of polyester and alkyd resins, which added to fiberglass reinforced plastics to make a strong, lightweight, and corrosion resistant material that is found in autos, boats, trucks, pipelines and electrical goods.

In secondary capacity, MA is added to drying oils to decrease the required drying time and enhances the coating quality of lacquers. Dispersants derived from MA prolong oil change intervals and enhance the efficiency of automotive engines. Fumaric and maleic acid are important MA derivatives used in paper sizing resins and as food and beverage acidulants (Lee, 2000).

The World Petrochemical (WP) reported that global production and consumption of MA in 2010 were approximately 1.7 million metric tons. Global capacity utilization was 65% in 2010, a slight increase from 2009. MA consumption is estimated to grow an average of 5.6 % per year from 2010 to 2015. Unsaturated polyester resins accounted for an estimated of 39% of global MA consumption in 2010, followed by 1,4-butandiol. Other application for MA include agricultural chemicals, malic acid, fumaric acid, lube oil additives, maleic anhydride-based copolymers, alkenyl succinic anhydrides, reactive plasticizers, sulfosuccinic acid esters, and a number of other specialty chemicals and organic intermediates (Sri Consulting, 2011).

2.2 Production of Maleic Anhydride

The first commercial process for MA production was by National Aniline and Chemical in 1982 using the Weiss and Downs process employing benzene as a raw material. In 1967, benzene-based process was favoured. With the development of petrochemical industry, benzene was available in larger quantities at lower prices. As a result, it became a more attractive raw material (Trivedi and Culbertson, 1982).

In 1971, Mitsubishi Chemical Industries first commercialized the MA process based on the oxidation of C_4 hydrocarbons. There is a stoichiometric advantage in using C_4 hydrocarbons over benzene since in the latter two carbons or one-third of the molecule is wasted. Thus, ideally 100 lb of benzene would yield 125.6 lb of MA whereas 100 lb of butane would yield 168.9 lb of

MA. This intrinsic advantage of C_4-hydrocarbon based raw material has shown greater activity for MA production in recent years. The using of butane as feedstock are gaining favour as the price of benzene climbs steeply and environmental regulations for benzene take effect (Trivedi and Culbertson, 1982).

The initial choice were butenes and butadienes because they were more highly reactive than *n*-butane. Butenes and butadienes were inexpensive and available worldwide. However, it was realised that the more viable route involved the use of *n*-butane as raw material. Three factors made it difficult to choose the better route. The first factor was some of the drawbacks were hardly recognised because only small amounts of by-products were obtained in the lab. The by-products include organic acids, which can make it more difficult to be separated from the products and can cause corrosion downstream from the reactor. The second factor was impossible to ascertain that the catalyst with butane had a shorter lifetime than with *n*-butane at laboratory level. For industrial applications, a catalytic lifetime of at least six months is necessary. The third factor was referring to the paradox of catalysis. With butenes, the reactivity was higher and fewer steps were needed to obtain the product. On the other hand, higher selectivity and cleaner reaction was obtained with *n*-butane (Cavani and Trifirò, 1994).

2.2.1 Production Technology

Modern commercial processes for MA production are based on the selective gas phase oxidation of butane over vanadium-phosphorus oxide (VPO) catalysts, either in fixed or fluidized-bed reactors. Fixed bed is a well known technology where improvements in selectivity are only possible by improving the catalysts. The main drawback of fixed beds is that highly diluted conditions must be employed (less than 2 % of butane in air) to avoid flammability limits. Recycling the unconverted butane is therefore not economically feasible. The heat generation produces hot spots, increasing the probability of runaway reactions occurring. Thus, fluidized bed reactors are the preferred solution for large scale plants (Gascón et al., 2006). Most laboratory studies with VPO catalysts involve fixed bed microreactors with very small sample sizes (often in the tens of milligrams range) in order to maintain homogeneity of the reaction atmosphere in contact with the catalyst (Mallada et al., 2000).

Fluidized bed processes permit more efficient heat removal and a better temperature control, avoiding yield losses and catalyst degradation related with hot spots. Higher feed concentrations, up to 4% butane in air, are possible because the fluidized catalysts act as a flame arrester, quenching the free radicals. However, the rapid axial mixing of catalyst, associated with gas back mixing in fluidized bed reactors, produces selectivity losses by degradation of butane and MA (Gascón et al., 2006).

Recently, Dupont designed and operated a circulating fluidized bed reactor (CFB) to produce MA from *n*-butane, using a vanadyl pyrophosphate catalyst encapsulated in a silica shell. A fraction of the pyrophosphate was oxidized to the V^{5+} state from the V^{4+} state in an air fed fluidized bed regenerator. The oxidized vanadyl pyrophosphate was shuttled to a transport bed reactor with a high concentration of butane and oxygen, the gas carried out through the bed velocities of 0.8 m/s (Patience and Bockrath, 2010).

2.3 Vanadium Phosphate Oxide (VPO)

VPO have shown promising results as heterogeneous catalysts in the selective oxidation of *n*-butane to MA. This is the only selective gas phase alkane oxidation that has been commercialized. The catalyst used for the oxidation of *n*-butane to MA is the vanadyl pyrophosphate, $(VO)_2P_2O_7$ which is obtained from the vanadyl hydrogen phosphate precursor through a topotactic transformation as shown on Figure 2.2 (Dutta, 2005; Schiøtt and Jørgensen, 1993).

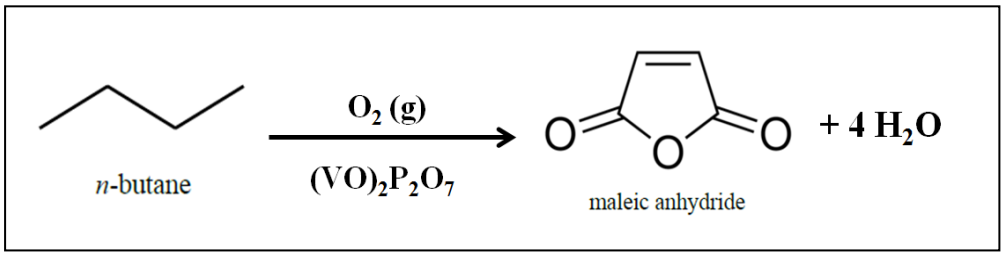

Figure 2.2: Oxidation reaction of *n*-butane to MA on a vanadyl pyrophosphate surface

Vanadium phosphates constitute a very interesting class of layered compounds which exists in a wide range of structural forms both due to the variable valency of vanadium as well as the large diversity in the bonding of VO_6 octahedron and the PO_4 structural units. The layered compounds held together by hydrogen bonding or weak van der waal's interaction (Dutta, 2005).

A series of oxidation reaction was outlined in Figure 2.3. The first step involved the hydrogen abstraction from *n*-butane giving 1-butene followed by further hydrogen abstraction with formation of 1,3-butadiene in which an 1,4-insertion of an electrophilic oxygen atom takes place producing 2,5-dihydrofuran. The 2,5-dihydrofuran is then further oxidized to an asymmetric lactone. MA is formed by a final oxidation of the remaining CH_2- group to a carbonyl group (Schiøtt and Jørgensen, 1993).

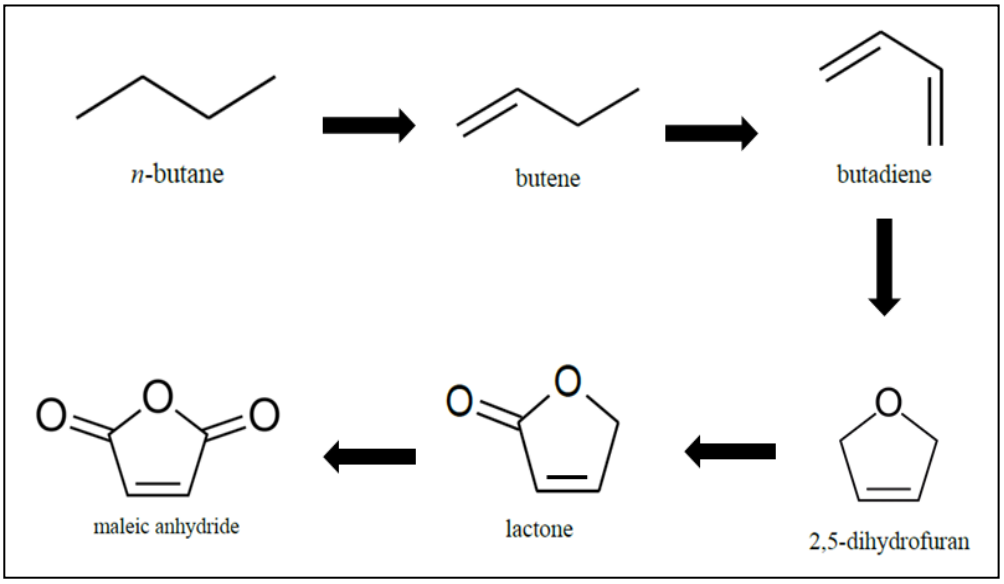

Figure 2.3: Reaction mechanism for the oxidation reaction of *n*-butane to MA

There are different VPO phases with vanadium in the +3, +4 and +5 oxidation states. The V(5+) phases correspond to hydrates like $VOPO_4.H_2O$, $VOPO_4.2H_2O$, phosphates $VOPO_4$ (α_I, α_{II}, β, γ, δ). The V(4+) phases correspond to hydrogenophosphates like $VOHPO_4.0.5H_2O$, $VOHPO_4.4H_2O$ or $VO(H_2PO_4)_2$, to pyrophosphate $(VO)_2P_2O_7$, to metaphosphates $VO(PO_3)_2$. The V(3+) phases correspond to VPO_4, $V(PO_3)_3$ (Bordes , 1987).

Vanadyl pyrophosphate, $(VO)_2P_2O_7$ is a well known catalyst for the C_4 oxidation to maleic anhydride (Centi et al., 1990). The reaction is due to the combined action of oxidative dehydrogenation and oxygenation on (1 0 0) surface plane of $(VO)_2P_2O_7$. The vanadyl dimer formed by vanadium ion coordinated to six oxygen lies on (1 0 0) plane which consists of fundamental structure of $(VO)_2P_2O_7$ and the oxygen ion double bonded in positions trans to vanadium ions (V=O) as shown in Figure 2.4 (Matsuura, 1992).

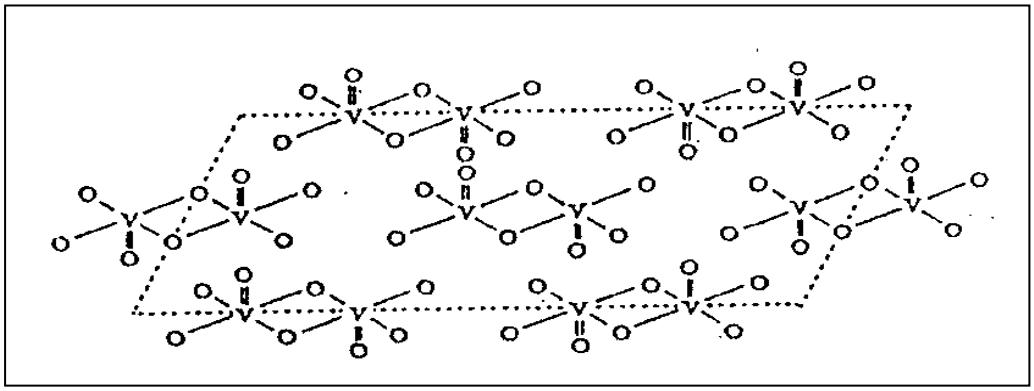

Figure 2.4: Basic (1 0 0) plane of $(VO)_2P_2O$

Vanadyl pyrophosphate system possesses sites able to perform the oxidative dehydrogenation of paraffins. This is demonstrated by the formation of benzene with high specificity from cyclohexane, as well as by the formation

of olefins and diolefins from cycloparaffins. Vanadyl pyrophosphate possesses centres able to perform great specificity with the allylic oxidation and able to insert oxygen into electron-rich substrates. Vanadyl pyrophosphate also possesses the ability to easily undergo reversible structural changes, from V (5+) to V (4+).

The oxidation state of vanadium under reaction conditions is a very important parameter in the control of the process selectivity. A certain number of oxidized vanadium sites are necessary to transform the intermediate olefins to the oxygenated products. An over oxidized surface may be responsible for the consecutives oxidative degradation of the desired products. Vanadyl pyrophosphate possesses acidic centres which able to perform a number of different transformation and favours bimolecular condensation reactions (Cavani and Trifirò, 1997).

2.3.1 Method of Preparation of VPO Catalysts

The catalytic properties of the $(VO)_2P_2O_7$ depends on the method by which the precursor is prepared (Shima and Hatano, 1997). The preparation of $(VO)_2P_2O_7$ via vanadyl hydrogen phosphate hemihydrate precursor can be classified into three general methods: (i) Aqueous method (VPA) (ii) Organic method (VPO) (iii) Dihydrate method (VPD) (Hutchings et al., 1997; Kiely et al., 1996). An alternative route via vanadyl hydrogen phosphate sesquihydrate precursor was developed by reducing the $VOPO_4.2H_2O$ in 1-butanol (Ishimura et al., 2000; Taufiq-Yap et al., 2004).

In aqueous synthesis, V^{V} compounds (V_2O_5) are reduced to V^{IV} in aqueous solutions of orthophosphoric acid, followed by the evaporation of solvent to dryness. (Equation 2.1)

$$V_2O_5 + 2NH_2OH\text{-}HCl + 2H_3PO_4 \rightarrow 2VOHPO_4 \cdot 0.5H_2O + N_2 + 2HCl + 4H_2O \quad \text{.....(2.1)}$$

In organic synthesis, V^{V} compounds (V_2O_5) are reduced by an anhydrous alcohol, followed by the addition of anhydrous orthophosphoric acid dissolve in the same alcohol and precipitation of $VOHPO_4 \cdot 0.5\ H_2O$. (Equation 2.2)

$$V_2O_5 + EtCHOHMe + 2H_3PO_4 \rightarrow 2VOHPO_4 \cdot 0.5H_2O + EtCOMe + 2H_2O \quad \text{..(2.2)}$$

In dihydrate synthesis, V^{v} orthophosphate dihydrate, $VOPO_4 \cdot 2H_2O$ is first synthesized from V_2O_5 and H_3PO_4 in aqueous medium and then reduced to $VOHPO_4 \cdot 0.5\ H_2O$ by an alcohol in a separate step as shown in equation (2.3) and (2.4):

$$V_2O_5 + 2H_3PO_4 + H_2O \rightarrow 2VOPO_4 \cdot 2H_2O + H_2O \quad \text{.....(2.3)}$$

$$2VOPO_4 \cdot 2H_2O + EtCHOHMe \rightarrow 2VOHPO_4 \cdot 0.5H_2O + EtCOMe + 3H_2O \quad \text{...(2.4)}$$

The use of an organic alcohol as a reducing agent instead of hydrochloric acid leads to the formation of a vanadyl phosphate ($VOHPO_4 \cdot \frac{1}{2} H_2O$) with the organic alcohol trapped between the layers forming the structure

of the phosphate. In all the catalysts prepared in an organic medium, the specific rate of *n*-butane oxidation is higher than that of the catalysts prepared in an aqueous medium. The organic alcohol trapped between the layers during its removal from the phosphate structure creates local modifications, inducing the formation of new active centres for the activation of *n*-butane, which is the rate-limiting step in the conversion of *n*-butane to MA reaction (Busca et al, 1986).

The catalyst prepared in the organic medium is more active than catalyst prepared in water. The difference in the preparation method resulted in a difference in the specific surface area of the catalyst, while the nature of the active sites was not affected by the preparation method. The surface area of the catalyst prepared in non-aqueous medium is in the range of 20-50 m^2/g, which is much higher than catalyst prepared in water (Shima and Hatano, 1997).

$(VO)_2P_2O_7$ synthesized via VPA method exists with a much higher irregular morphology while the crystalline $(VO)_2P_2O_7$ synthesized via VPO method adopts a regular oblong morphology exposing (1 0 0), (0 2 1) and (0 1 2) crystal faces. $(VO)_2P_2O_7$ prepared via VPD method shows a high surface area platelet morphology preferentially exposing (1 0 0) surfaces. The morphology displayed by $(VO)_2P_2O_7$ prepared via VPD method is approaching optimal as the (1 0 0) planes of $(VO)_2P_2O_7$ has shown to have best catalytic properties for MA formation (Kiely et al., 1996).

Ishimura et al (2000) reported that vanadyl hydrogenphosphate sesquihydrate calcined at 480 °C over 10 hours on stream revealed high specific activity per unit surface area in the vapour-phase oxidation of *n*-butane. Using 1-butanol as solvent, the sesquihydrate could be intercalated with cobaltous acetate to afford modified $(VO)_2P_2O_7$ with high activity, but both selectivity to MA and surface area decreased with increasing cobalt-contents. Intercalated additives retarded topotactic dehydration of layered precursor to afford the crystalline active species, leading to an increase in the unfavourable combustion activity due to pentavalent β-$VOPO_4$ species.

2.3.2 Factors Affecting the Performance of Catalyst

Thermal treatment conditions of precursor such as environment, temperature and duration is one of the most important factors affecting the performance of vanadyl pyrophosphate catalysts (Rownaghi et al., 2009). Two different activation procedures are generally reported in previous studies: (i) activation in an oxygen-free atmosphere at temperature greater than 673K, followed by introduction of the reactant mixture of *n*-butane in air. $VOHPO_4 \cdot 0.5H_2O$ transforms quantitatively to poorly crystalline $(VO)_2P_2O_7$ during the first step, which can be partially oxidized to V^v orthophosphates after the introduction of the reactant mixture; (ii) calcination in air at $T < 673K$, after which the reactant mixture is introduced (Gulliants and Carreon, 2005).

2.3.2.1 Activation Duration

The active phase is generally generated by a long-term calcination of the precursor (Taufiq-Yap and Saw, 2008). During prolonged time on stream, changes occur in both the catalytic behaviour and physiochemical properties of the catalyst. A catalyst after a prolonged period of time on stream is termed as "equilibrated" catalyst while a fresh catalyst is termed as "non-equilibrated" catalyst. A non-equilibrated catalyst is more active and has lower selectivity in MA, especially at high conversion rates. V^{4+} is more easily oxidized to V^{5+} because the reactant mixture becomes more oxidizing as a result of the considerable decrease in *n*-butane concentration (Cavani and Trifirò, 1994).

Precursors activated for a period less than 100 hours will yield the so-called "non-equilibrated" catalysts, while a calcination time of more than 1000 hours will yield the "equilibrated" catalysts, which were thermodynamically more stable under usual reaction conditions. The equilibrated catalyst is more active in the oxidation of *n*-butane. The higher activity can be contributed to its higher specific surface area. It possesses surface sites that are specific in the oxidation of *n*-butane to MA, thus yielding the desired product with a higher selectivity (Albonetti et al., 1996).

A general interpretation for the evolution of the catalysts during the activation process under *n*-butane/air mixture was proposed. First the precursor would be in part transformed into $(VO)_2P_2O_7$ via the usually invoked topotactic process (3) and in part oxidized into δ-$VOPO_4$. Both phases are very poorly

crystallized at 400 °C. The activation time will mainly induce the progressive reduction of δ-$VOPO_4$ into $(VO)_2P_2O_7$ and also the transformation of δ-$VOPO_4$ into α_{II}-$VOPO_4$ (Abon et al., 1995). This evolution of the catalysts is shown schematically in Figure 2.5.

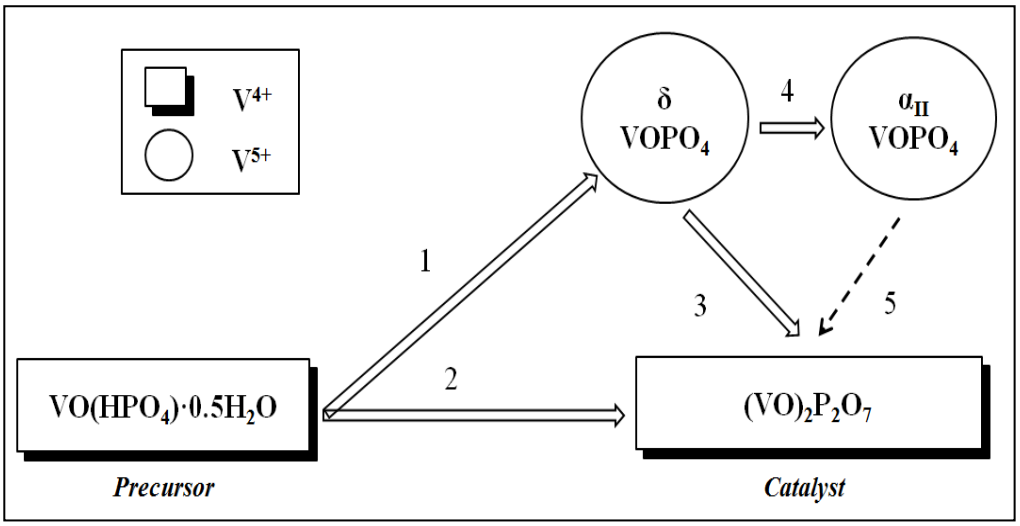

Figure 2.5: Scheme of the proposed evolution of the VPO catalyst with activation time: (1) Oxydehydration; (2) Topotactic transformation; (3) and (5) Reduction of V^{5+} to V^{4+}; and (4) Isovalence transformation

Taufiq-Yap et al. (2001) reported that increasing the calcinations duration of the catalysts prepared via organic route led to the complete removal of $VOPO_4$ phase from the catalyst VPO 100 and VPO 132, but seen as a minor component for the catalyst VPO 40. The longer pre-treatment was reported to produce catalysts with increasing amount of characteristic rosette-type agglomerate. Increasing the length of time of pre-treatment of vanadyl pyrophosphate catalysts increases the surface area of the catalyst and change the surface and bulk morphologies into one in which more oxygen can be removed from the lattice by reaction with H_2.

2.3.2.2 Activation Temperature

Poli et al (1981) reported that at activation temperature about 380 °C, the temperature at which $(VO)_2P_2O_7 \cdot 2H_2O$ losses water, transformations take place which lead to different compounds, depending on the activation atmosphere and the P/V ratio.

Variation in calcination temperatures were reported to have an important effect on the properties of the vanadium-antimony oxide as an increase in calcination temperature produce more aggregated solids with small surface area value as compared to sample activated at low temperature (Irmawati et al., 2004).

2.3.2.3 Activation Environment

Cheng and Wang (1997) reported that calcination atmosphere affects the catalyst morphology and vanadium valence. The vanadium valence increased and achieved the optimised MA yield as the oxidizing potential of the gas increase. However, the surface area decreased with the oxidizing strength of the calcinations atmospheres. SEM revealed that the size of the platelet face decrease with the oxygen concentration used in the calcinations increase. Small platelet face formed when activated in higher oxygen concentrations could facilitate the oxygen diffusion, making the catalyst oxidation faster and thus increase the vanadium valence of the catalyst. An unpromoted catalyst was more resistant to oxidation than the promoted catalyst in the calcination (Cheng

and Wang, 1997).

Different calcination agents influence the catalytic performance of the VPO catalysts (Taufiq-Yap and Saw, 2008). Taufiq-Yap and Saw (2008) revealed that n-butane/ air calcined catalysts gave higher surface area and higher conversion rate compared to propane/ air activated catalysts. Calcination in nitrogen causes the loss of water and the transformation of hemihydrate to pyrophosphate (Guliants et al., 1995).

2.3.2.4 Addition of Promoters

The catalytic performance of VPO catalysts can be enhanced by the addition of promoters. Industrial catalysts contain different kinds of promoters including cations such as Ce, Cd, Ni, Zn, Bi, Cu, Li, V, Zr, Mg, Ti, La, Mo, Nb, B, Fe and Cr which were reported in patents (Cornaglia et al., 2000). Promoters have a twofold structural role: (i) to enable the formation of the required VPO compounds and decrease the formation of deleterious phases; (ii) to enable the formation of solid solutions that regulate the catalytic activity of the solid (Hutchings, 2001).

Zazhigalov et al. (1996) studied the mechanism by which the introduction of alkali and alkali-earth metal ions to the VPO catalyst. Zazhigalov et al. (1996) reported that the introduction of Mg, Ca and Ba increase the selectivity to MA while the addition of Na, K and Cs increase the rate of alkane oxidation. The preparation of catalysts with high activity in

butane oxidation and high selectivity to maleic anhydride requires a fine tuning of the basicity of surface oxygen atoms to accelerate the activation of butane (Zazhigalov et al., 1996).

Brutovsky et al. (1996) reported that the catalysts incorporated with Mg, Ca and Ba ions provide a higher conversion of butane, selectivity and yield of maleic anhydride compared to unpromoted catalysts. Selectivity of MA increases as the natural basicity of the added promoters, from Mg to Ba increase (Brutovsky et al., 1996). The increase in the strength of the basic centres at the surface of the VPO catalysts results in the firmer bonding of acidic products (MA) at the catalyst surface (Brutovsky et al., 1996).

Pierini and Lombardo (2005) reported that the chromium, molybdenum and tungsten were selected as promoters because they have “d” character, various oxidation states under reaction conditions, their oxides are acidic and they form intercalation or substitution compounds with vanadium. In fact, these elements were important in accelerating the rate determining step of C-H bond breaking.

Govender et al. (2004) revealed that cobalt promoted catalyst improves the selectivity towards MA. Cobalt stabilizes the phosphorus in the lattice of the catalyst and reduces or prevents the sublimation of phosphorus under the high-operating temperatures around 673K where excess catalyst is required for selective oxidation of n-butane (Govender et al., 2004). Cobalt could be intercalated with cobaltous acetate to afford the modified $(VO)_2P_2O_7$ with high

activity but low selectivity to MA and decreased in surface area with increasing cobalt content (Ishimura et al., 2000).

Taufiq-Yap et al. (2006) reported that the addition of Bismuth into the lattice of a vanadyl pyrophosphate catalyst enhance the activity of the catalysts since the catalyst posses highly active and labile lattice oxygen. The reactive and labile oxygen species originated from the V^{4+} are capable of increasing the rate of C-H bonding (Taufiq-Yap, 2006). Goh et al. (2008) reported that the oxygen species associated with the V^{4+} played an important role in the activity of the catalyst while the oxygen species linked to V^{5+} involved in the formation of maleic anhydride. Goh et al. (2008) reported that the simultaneous addition of BiFe oxide powder in the course of the synthesis of precursor gave higher intrinsic activity although it had lower surface area. This may be due to higher amount of oxygen species removed associated with V^{4+} which occurred at lower temperature (Goh et al., 2008).

Pries de Oliveira et al (2000) proposed that niobium phosphate (NbPO) enhance the catalytic performance for *n*-butane oxidation to maleic anhydride and strong improvement of the activation time of the VPO precursor. Sartoni et al. (2004) studied the effect of Gallium doping using different Gallium source, which were gallium oxide, gallium phosphate and gallium acetylacetonate. Ga^{3+} promotes the activity of VPO catalyst and the best source was gallium acetylacetonate (Sartoni et al., 2004).

Rownaghi et al. (2009) revealed that the addition of rare-earth element gives rise to the formation of $VOPO_4$ and $(VO)_2P_2O_7$ phases which promote the catalyst performance and ensures that the deleterious phases such as $VO(H_2PO_4)_2$, are not formed.

Chapter 3

Materials and Methodology

3.1 Materials and Gases

Table 3.1: List of reagents for synthesis and characterisation of VPS catalysts

Reagent	Supplier
Vanadium (V) Pentoxide, V_2O_5 (≥ 99.0 %)	Merck
Ortho-Phosphoric Acid, *o*-H_3PO_4 (85 %)	Merck
1-butanol, $CH_3(CH_2)_3OH$ (99.5 %)	Merck
Sulphuric Acid, H_2SO_4 (95-97 %)	Merck
Potassium Permanganate, $KMnO_4$ (≥ 99.0 %)	Fischer Scientific
Ammonium Iron (II) Sulphate Hexahydrate, $(NH_4)_2Fe(SO_4)_2.6H_2O$ (≥ 99.0 %)	Fischer Scientific
Barium nitrate, $Ba(NO_3)_2$ (≥ 99.0 %)	Merck
Diphenylamine, $C_{12}H_{11}$ (≥ 99.0 %)	Acros Organics
Magnesium nitrate hexahydrate, $Mg(NO_3)_2.6H_2O$ (≥ 99.0 %)	Merck
Calcium nitrate tetrahydrate, $Ca(NO_3)_2.4H_2O$ (≥ 99.95 %)	Merck
Strontium nitrate, $Sr(NO_3)_2$ (≥ 99.99 %)	Merck

Table 3.2: List of gases for activation and characterisation of VPS catalysts

Gases	Supplier
1% Oxygen in Nitrogen	MOX-LINDE SDN. BHD
5.55% Helium in Hydrogen	MOX-LINDE SDN. BHD
Purified Compressed Air	MOX-LINDE SDN. BHD
99.99% Purified Argon	MOX-LINDE SDN. BHD
99.99% Purified Helium	MOX-LINDE SDN. BHD
99.99% Purified Nitrogen	MOX-LINDE SDN. BHD
99.8% Purified Oxygen	MOX-LINDE SDN. BHD

Table 3.3: List of sample denotation

Sample	Denotation
Bulk VPS catalyst activated for 6 hours	VPS-6
Bulk VPS activated catalyst for 18 hours	VPS-18
Bulk VPS activated catalyst for 30 hours	VPS-30
Bulk VPS activated catalyst for 75 hours	VPS-75
1 mol% Ba-doped VPS catalyst activated for 6 hours	VPS-Ba-6
1 mol% Ba-doped VPS catalyst activated for 18 hours	VPS-Ba-18
1 mol% Ba-doped VPS catalyst activated for 30 hours	VPS-Ba-30
1 mol% Ba-doped VPS catalyst activated for 75 hours	VPS-Ba-75
3 mol% Mg-doped VPS catalyst activated for 6 hours	VPS-Mg
3 mol% Ca-doped VPS catalyst activated for 6 hours	VPS-Ca
3 mol% Sr-doped VPS catalyst activated for 6 hours	VPS-Sr

3.2 Preparation of the Precursor

3.2.1 Preparation of the Bulk Precursor

The synthesis of the sesquihydrate precursor was divided into two stages, involving vanadyl phosphate dihydrate, $VOPO_4 \cdot 2H_2O$ as an intermediate.

In the first stage (Figure 3.1), 90 mL of 85 % *o*-H_3PO_4 was added to 360 mL of distilled water with 15g of V_2O_5. The mixture was then stirred under reflux at 393K for 24 hours. The brownish solid solution changed gradually to yellow colour. The resultant yellow solid ($VOPO_4 \cdot 2H_2O$) was then recovered via centrifugation and oven dried at 353K.

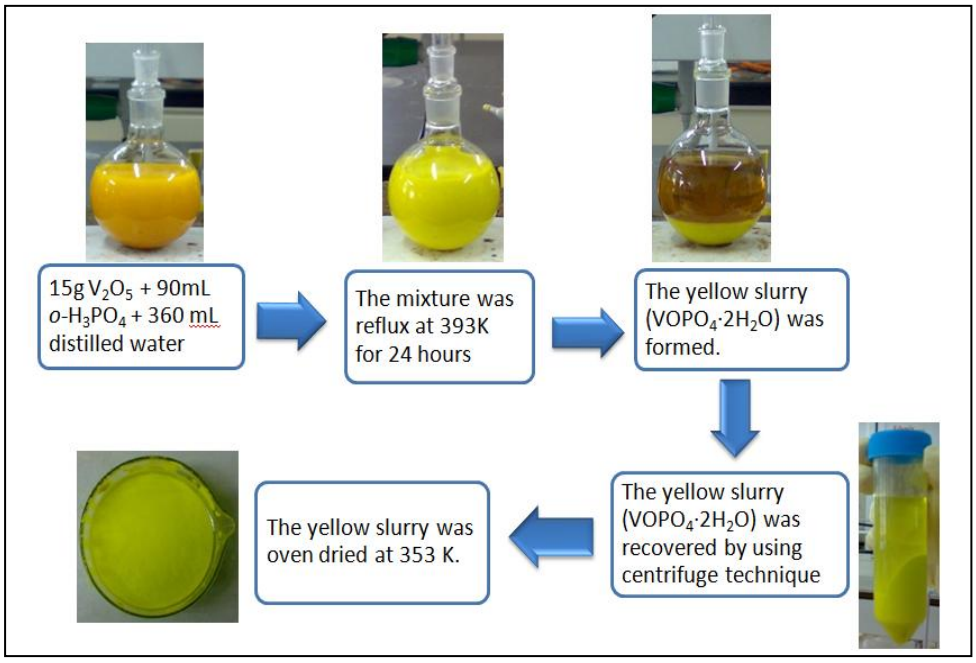

Figure 3.1: Preparation of Vanadyl phosphate dihydrate, $VOPO_4 \cdot 2H_2O$

In the second stage (Figure 3.2), 10.0g of $VOPO_4 \cdot 2H_2O$ obtained from the first stage was added to 233 mL of 1-butanol. The mixture was then stirred under reflux at 373 K for 8 hours and whitish blue precipitate was obtained. The whitish blue precipitate ($VOHPO_4 \cdot 1.5H_2O$) was then recovered via centrifugation and oven dried at 353K.

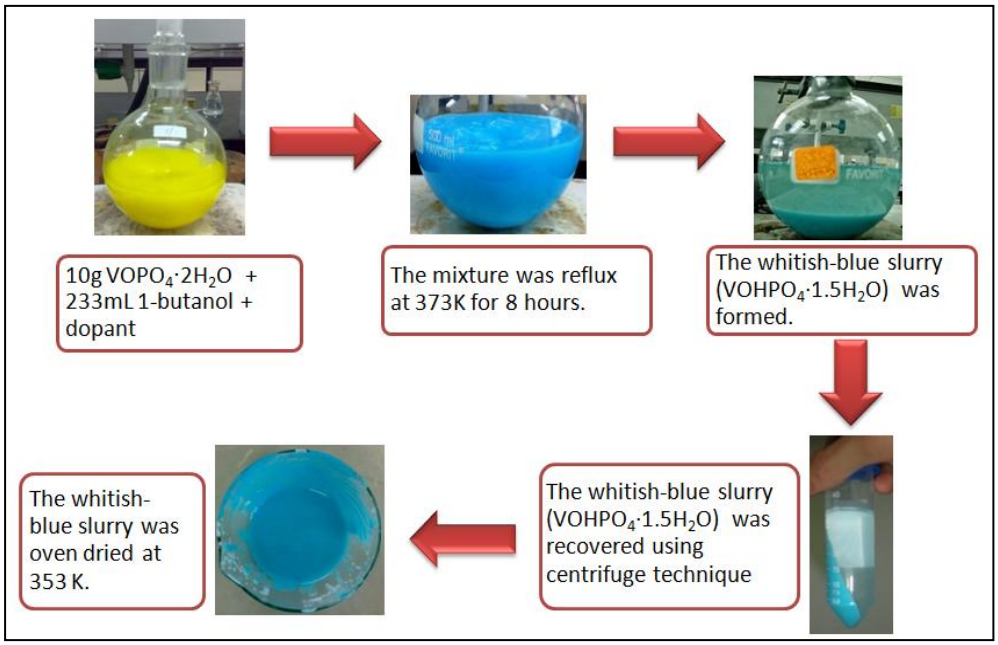

Figure 3.2: Formation of Vanadyl hydrogen phosphate sesquihydrate, $VOHPO_4 \cdot 1.5H_2O$

The whitish blue powder obtained from the second stage was activated at 733 K in a reaction flow of 1% oxygen in nitrogen (1% O_2/N_2) for 6, 18, 30 and 75 hours (Figure 3.3). The activated catalysts were denoted as VPS-6, VPS-18, VPS-30 and VPS-75.

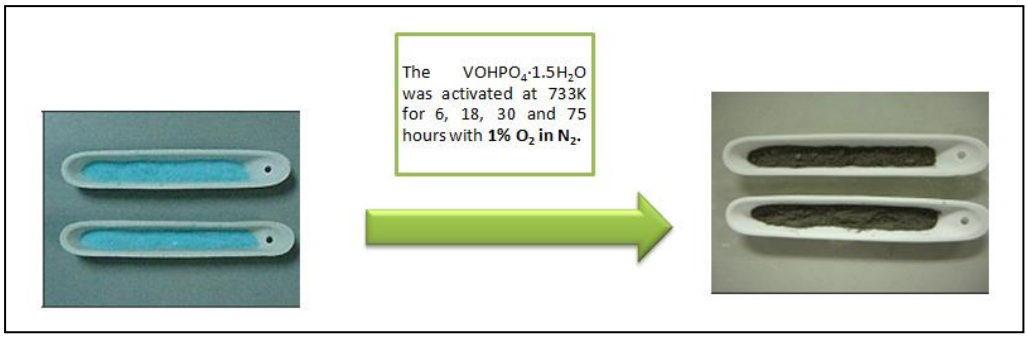

Figure 3.3: Activation of $VOHPO_4 \cdot 1.5H_2O$ in 1 % oxygen in nitrogen at 733K

3.2.2 Preparation of 1 % Barium-Doped Precursor

In the first stage, 90 mL of 85 % *o*-H_3PO_4 was added to 360 mL of distilled water with 15g of V_2O_5. The mixture was then stirred under reflux at 393K for 24 hours. The brownish solid solution changed gradually to yellow colour. The resultant yellow solid ($VOPO_4 \cdot 2H_2O$) was then recovered via centrifugation and oven dried at 353K.

In the second stage, 10.0g of $VOPO_4.2H_2O$ obtained from the first stage was added to 233 mL of 1-butanol. The dopant, 1 % (0.132g) of $Ba(NO_3)_2$ was dissolved in the mixture and stirred under reflux at 373 K for 8 hours. The whitish blue precipitate ($VOHPO_4 \cdot 1.5H_2O$) was obtained and recovered via centrifugation, followed by oven dried at 353K. The whitish blue powder obtained from the second stage was activated at 733 K in a reaction flow of 1% O_2/N_2 for 6, 18, 30 and 75 hours. The activated catalysts were denoted as VPS-Ba-6, VPS-Ba-18, VPS-Ba-30 and VPS-Ba-75, respectively.

3.2.3 Preparation of 3% Magnesium, Calcium and Strontium-Doped Precursor

In the first stage, 90 mL of 85 % *o*-H_3PO_4 was added to 360 mL of distilled water with 15g of V_2O_5. The mixture was then stirred under reflux at 393K for 24 hours. The brownish solid solution changed gradually to yellow colour. The resultant yellow solid ($VOPO_4 \cdot 2H_2O$) was then recovered via centrifugation and oven dried at 353K.

In the second stage, 10.0g of $VOPO_4 \cdot 2H_2O$ obtained from the first stage was added to 233 mL of 1-butanol. Respective amount of the $Mg(NO_3)_2.6H_2O$, $Ca(NO_3)_2.4H_2O$ and anhydrous $Sr(NO_3)_2$ were dissolved in the mixture to synthesise the 3 mol % Mg/V, Ca/V and Sr/V, respectively. The mass for each dopant used in the catalysts synthesis was summarised in Table 3.4. The mixture was then stirred under reflux at 373 K for 8 hours and a whitish blue precipitate was obtained. The whitish blue precipitate ($VOHPO_4 \cdot 1.5H_2O$) was then recovered via centrifugation and oven dried at 353K. The whitish blue powder obtained was activated at 733 K in a reaction flow of 1% O_2/N_2 for 6 hours. The activated catalysts were denoted as VPS-Mg, VPS-Ca and VPS-Sr, respectively.

Table 3.4: The mass for each mole percentage of dopants used in the synthesis of catalysts

Mole Percentage of Metal/Vanadium (M/V)	Mass (g)
1 mol % Ba/V	0.3120
3 mol % Mg/V	0.3886
3 mol % Ca/V	0.3579
3 mol % Sr/V	0.3207

3.3 Characterisation Techniques

Different characterisation techniques have been carried out to analyse the synthesised catalysts. Physical analyses including X-Ray Diffraction (XRD), BET Specific surface area analysis, Temperature-Programmed Desorption, Reduction and Oxidation (TPDRO) and Scanning Electron Microscope with Energy dispersive X-ray (SEM-EDX). Chemical analyses were carried out using redox titration and Inductive Coupled Plasma-Optical Emission Spectrometer (ICP- OES). Catalytic analysis was carried out in a fixed-bed flow micro reactor.

3.3.1 X-Ray Diffraction (XRD)

The X-ray diffraction analysis was carried out using Shimadzu diffractometer (LabX XRD- 6000) employing CuKα Philips glass diffraction X-ray tube with broad focus of 2.7 kW on the sample at ambient temperature. The basal spacing was determined via powder technique. The samples was placed on the middle of the well and pressed flat with a glass slide. The top of the sample must be coplanar with the top of the aluminium sample holder.

The X-ray diffractometer analyse crystalline states under normal atmospheric conditions. This method is non-destructive. X-rays focused on the sample fixed on the axis of the spectrometer (goniometer) are diffracted by the sample. The changes in the diffracted X-ray intensities were measured and plotted against the rotation angles of the sample. The result is referred to as the X-ray diffraction pattern of the sample.

3.3.2 BET Specific Surface Area Analysis

The BET specific surface area analysis was carried out using *Thermo Electron Sorptomatic 1990*. The specific surface area was calculated with BET method. Brunauer, Emmett and Teller derived the equation for physical adsorption of gases on solid surfaces that leads to multilayer adsorption.

The first weighing, W_1 was carried out with the outgassed burette under vacuum without the sample. Then, 0.5 g of the sample catalyst was transferred into the burette. The second weighing, W_2 was carried out with the outgassed burette under vacuum with sample inside. The real weight of the sample was obtained by subtraction of two weightings (W_2-W_1). Sample pre-treatment was the combined operation of vacuum and temperature to remove the humidity from the sample. This operation was carried out using the outgassing stations and furnaces located on the front of the instrument. The sample was treated at 393 K for 1 hour.

The blank measurement was a fast analytical run which determine the dead space of the tubing and sample holder not occupied by the sample. A blank measurement was performed using Helium gas. The pre-treatment was carried out again after the blank measurement. Then, the analysis measurement was carried out by using nitrogen gas. The specific surface area of the sample was determined by using BET method.

3.3.3 Redox Titration

The average oxidation states of vanadium for the catalysts were determined by redox titration according to a method reported by Niwa and Murakami (Niwa and Murakami, 1982). Firstly, 0.1 g of the sample was dissolved in 2 M sulphuric acid and titrated with 0.01 N potassium permanganate solutions to oxidise both the V^{3+} and V^{4+} in the solution to V^{5+}. The colour changed from greenish blue to pink indicated that the end point was reached. The volume of potassium permanganate solution used was recorded as V_1. Then, a few drops of indicator, diphenylamine, were added into the oxidised solution. The oxidised solution was then titrated with 0.01N ammonium iron (II) sulphate solution to reduce the V^{5+} to V^{4+}. The end point was confirmed by the colour change of the solution from deep purple to greenish blue. The volume of ammonium iron (II) sulphate solution used was denoted as V_2. A few drops of diphenylamine (indicator) was added to the 25 mL of the fresh catalysts solution and titrated with 0.01 N ammonium iron (II) sulphate solution in order to determine the V^{5+} present in the catalysts. The end point was determined by the colour changed of the solution from purple to

greenish blue. The volume of ammonium iron (II) sulphate solution used was recorded as V_3.

According to Niwa and Murakami,

$(V^{4+} + 2V^{3+})\ (V_a) = 20\ [MnO_4^-]\ (V_1)$……(3.1)

$(V^{3+} + V^{4+} + V^{5+})\ (V_b) = 20\ [Fe^{2+}]\ (V_2)$……(3.2)

$(V^{5+})\ (V_c) = [Fe^{2+}]\ (V_3)$……(3.3)

Where V^{3+}, V^{4+}, and V^{5+} are the concentration of vanadium at different oxidation states; $[MnO_4^-]$ is the concentration of potassium permanganate solution; $[Fe^{2+}]$ is the concentration of ammonium iron (II) sulphate solution; V_1 is the volume of potassium permanganate solution used; V_2 and V_3 are the volume of ammonium iron (II) sulphate solution used; V_a, V_b, and V_c are the volume of the respective catalysts solution used. (Equation 3.1, 3.2 and 3.3)

The average oxidation state of vanadium (AV) was showed in equation 3.4:

$$V_{AV} = \frac{3V^{3+} + 4V^{4+} + 5V^{5+}}{V^{3+} + V^{4+} + V^{5+}} \quad \text{……(3.4)}$$

3.3.4 Temperature-Programmed Desorption, Reduction, and Oxidation (TPDRO)

TPDRO analysis provides the determination of the energies involved in the chemisorptions and desorption processes of the reactants and products. The detector is a TCD type (dynamic flow method), which makes this instrument extremely sensitive, providing the solution for a large range of linearity. The complete characterization sequence of an active solid generally consists of two separate phases: the pre-treatment and the analysis.

3.3.4.1 Temperature Programmed Reduction (TPR) Analysis

TPR analysis was carried out using *Thermo Electron TPDRO Series 1100*. The sample was weighed and placed in the reactor between two layers of quartz wool. The internal volume reducer was used to firmly close the reactor. The reactor was then assembled to the TPDRO. Prior to analysis, the catalysts were pretreated in a vacuum oven to remove the unwanted adsorbates from the catalyst surface. The sample was cleaned by heating it to 473 K (10 K/ min) in a nitrogen flow (25cm^3/ min) and holding it to that flow at 473 K for 30 minutes before cooling to room temperature. Then, the flow was switched to 5.55 % H_2/ N_2 (25cm^3/ min) and the temperature was raised to 1173 K (5 K/ min) following the conductivity of the eluted gas. TPR profile was obtained as a plot of the hydrogen consumption of the sample against the time, which was converted to a function of temperature.

3.3.4.2 Temperature Programmed Desorption (TPD) Analysis

TPD analysis was carried out using *Thermo Electron TPDRO 1100*. The sample was weighed and placed in the reactor between two layers of quartz wool. The internal volume reducer was used to firmly close the reactor. The reactor was then assembled to the TPDRO. The pre-treatment process was initiated by heating the sample at 673 K in an oxygen flow (1 bar, 25 cm^3 min^{-1}) and holding at 673 K for 30 minutes before cooling it to ambient temperature. Analysis was then started by switching the flow to helium gas (1 bar, 25 cm^3 min^{-1}), and the temperature was raised to 1173 K. The desorbed molecules from the surface of the sample were swept by the carrier gas to the thermal conductivity and quantified detector. The change in the thermal conductivity detector for the gas mixture before and after reaction is measured. TPD spectrum was obtained as a plot of the amount of adsorbate desorbed against the temperature.

3.3.5 Scanning Electron Microscope-Energy Dispersive X-Ray (SEM-EDX)

The morphology and elemental composition of the catalysts were determined using the Hitachi S-3400N instrument equipped with EDAX software. A small amount of the sample was placed on the surface of a carbon tape, which had been fixed on an aluminium stub (diameter 10 mm). SEM analysis images a sample by scanning it with a high-energy beam of electrons. The electrons interact with the atoms that make up the sample producing signals that contain information about the sample's surface topography,

composition, and other properties such as electrical conductivity. For EDX characterization, the atoms on the surface of the catalyst powders are excited by the electron beam from the SEM, emitting specific wavelengths which are characteristic of the atomic structure of the elements.

3.3.6 Inductive Coupled Plasma-Optical Emission Spectroscopy (ICP- OES)

Chemical analyses were performed on a Perkin-Elmer ICP-OES Optima 7000 DV. The molar ratio, P/V was determined using this technique. A known amount of catalyst (0.025 g) was digested in 10 mL of 8 M HNO_3 with slight heating and continuous stirring. The resulting solutions were diluted with distilled water to give nominal concentration in the range of 100–120 ppm. The standard solution of phosphorus was prepared in the concentration of 10, 20 and 30 ppm while standard solution of vanadium was prepared in the concentration of 10, 20, 30 and 40 ppm. The standard solutions of Mg^{2+}, Ca^{2+} and Sr^{2+} were prepared in concentrations of 1.0, 2.0, 3.0, 4.0 and 5.0 ppm while the standard solution of Ba^{2+} was prepared in the concentration of 0.5, 1.0, 1.5, 2.0 and 2.5 ppm. Distilled water was used as a blank solution, *i.e.* the control. All the standard and blank solutions were added with 10 mL of 8 M HNO_3 in order to be consistent with the sample solutions.

3.3.7 Catalytic Testing

The oxidation of *n*-butane was carried out in a fixed-bed continuous flow micro reactor at 673 K with GHSV of 2400 h^{-1} containing 250 mg of catalyst. A mixture of 1.0% *n*-butane and air was fed to the reactor via calibrated mass flow controller. The products were then fed via heated lines to an on-line gas chromatography for analysis. The reactor comprised a stainless steel tube with the catalyst held in place by plugs of quartz wool. A thermocouple was located in the center of the catalyst bed and temperature control was typically ± 1 K. Carbon mass balances of ≥ 95 % were typically observed.

Chapter 4

Results and Discussion

4.1 Effect of Activation Duration for Bulk and Ba-doped VPS Catalysts

4.1.1 X-Ray Diffraction (XRD)

The powdered XRD pattern for the bulk VPS catalysts activated at 733 K under a flow of 1% O_2/N_2 for 6, 18, 30 and 75 hours are shown in Figure 4.1. XRD pattern showed diffraction pattern comprised of a well-crystallised $(VO)_2P_2O_7$ phase. Three main characteristic peaks observed at 2θ= 22.8°, 28.4° and 29.8° (JCPDS File No. 34-1381), which corresponds to (0 2 0), (2 0 4) and (2 2 1) planes, respectively.

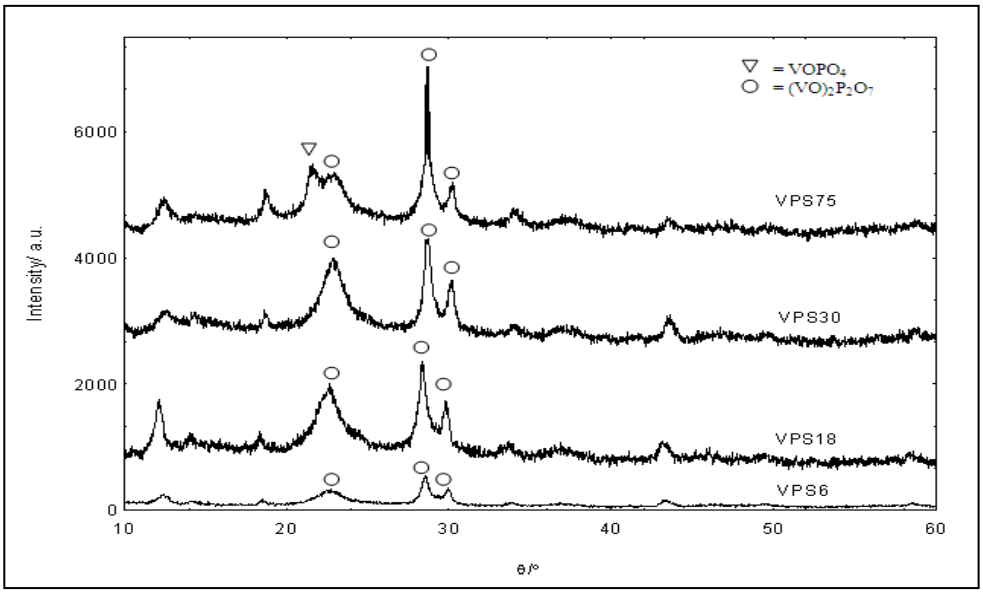

Figure 4.1: Powdered XRD pattern for the bulk VPS catalysts

The increase of activation duration from 6 to 30 hours led to the major reflection peaks being more intense and narrower width size, which indicated an enhanced formation of V^{4+} phase, *i.e.* $(VO)_2P_2O_7$. The result obtained was different from previous studies, which reported that increase in activation duration for VPS catalysts calcined in 0.75 % *n*-butane/air had increased the intensity of the peak at 2θ= 22.8° but decreased the intensity of the peak at 2θ= 28.4° (Taufiq-Yap et al., 2004).

However, as the activation duration was increased to 75 hours, VPS-75 was found to consist of a mixture of $(VO)_2P_2O_7$ and a V^{5+} phase, *i.e.* $VOPO_4$ (JCPDS File No. 27-0948) observed at 2θ= 21.4°. This indicated that increasing activation duration in 1% O_2/N_2 would enhance the formation of V^{5+} phase. This may be due to the over oxidation of the VPS-75 catalyst, which causes the V^{4+} phase to be oxidized to V^{5+} phase. Previous studies reported that for the VPS catalysts calcined in 0.75 % *n*-butane/air via the same synthetic route for 75 hours, the $VOPO_4$ peak emerged at 2θ= 29.3° (Taufiq-Yap et al., 2004). Only equilibrated catalysts, *i.e.* catalysts that had been activated for at least 200 hours, undergo complete vanadium reduction and formed stable V^{4+} phase (Cavani and Trifirò, 1994).

The powdered XRD pattern for the 1 mol % Ba-doped VPS catalysts activated at 733 K under a flow of 1% O_2/N_2 for 6, 18, 30 and 75 hours are shown in Figure 4.2. XRD pattern showed similar diffraction pattern comprised of a well-crystallised $(VO)_2P_2O_7$ phase with three main characteristic peaks

observed at 2θ= 22.8°, 28.4° and 29.8° (JCPDS File No. 34-1381), corresponding to (0 2 0), (2 0 4) and (2 2 1) planes, respectively.

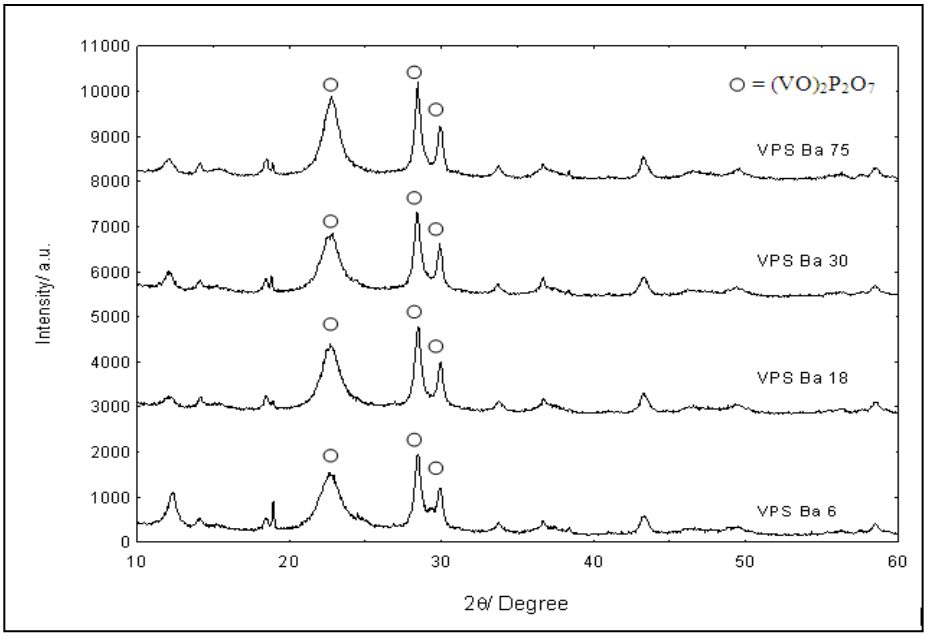

Figure 4.2: Powdered XRD pattern for the Ba-doped VPS catalysts

The intensity of the three major peaks (2θ= 22.8°, 28.4° and 29.8°) for all Ba-doped VPS catalysts was not markedly affected by the increasing activation duration. There was no additional V^{5+} peak detected for VPS-Ba-75 as seen in bulk VPS-75. This could be rationalised that the amount of this particular V^{5+} phase was below the detectable limit of XRD.

As tabulated in Table 4.1, the crystallite size of (0 2 0) plane for the VPS-6, VPS-18, VPS-30 and VPS-75 were calculated as 38.12 Å, 45.22 Å, 52.41 Å and 56.88 Å, respectively, whereas the crystallite size for (2 0 4) reflection plane were calculated as 117.56 Å, 124.45 Å, 138.16 Å and 106.61 Å, respectively. The increased in activation duration have shown to produce

catalysts with larger crystallite sizes in the (0 2 0) direction. This trend was found to be similar as that obtained for catalysts prepared via the same route but with a different activation environment *i.e.* 0.75 % *n*-butane/air. The only difference is that the line width obtained for 1% O_2/N_2 activated catalysts were relatively higher, indicating the presence of VPS catalysts with lower crystallite sizes for both (0 2 0) and (2 0 4) reflection planes (Taufiq-Yap et al., 2004).

Table 4.1
XRD data for the bulk and Ba-doped VPS catalysts

Catalysts	Line width [a] (020) (°)	Line width [b] (204) (°)	Crystallite Size [c] (020) (Å)	Crystallite Size [c] (204) (Å)
VPS-6	2.1000	0.6889	38.12	117.56
VPS18	1.7710	0.6508	45.22	124.45
VPS-30	1.5282	0.5868	52.41	138.16
VPS-75	1.4088	0.7603	56.88	106.61
VPS-Ba-6	1.7477	0.7080	45.82	114.40
VPS-Ba-18	1.4230	0.6638	56.28	122.00
VPS-Ba-30	1.4139	0.6736	56.64	120.22
VPS-Ba-75	1.2586	0.6870	63.63	117.93

Calculation for crystallite size was showed in Appendix C.
[a] FWHM of (020) reflection
[b] FWHM of (204) reflection
[c] Crystallite thickness by means of Scherrer's formula

The line width of Ba-doped VPS catalysts for (0 2 0) reflection plane decreased as the activation duration increased, indicating the increasing crystallite size from VPS-6 to VPS-75. The crystallite size of (0 2 0) plane for the VPS Ba-6, VPS Ba-18, VPS Ba-30 and VPS Ba-75 were calculated as 45.82 Å, 56.28 Å, 56.64 Å and 63.63 Å, respectively, whereas the crystallite size for (2 0 4) reflection plane were calculated as 114.40 Å, 122.00 Å, 120.22 Å and 117.93 Å, respectively (Table 4.1).

The trend obtained for Ba-doped VPS catalysts was found to be similar as obtained for bulk VPS catalysts. The only difference is that the crystallite size obtained for Ba-doped VPS catalysts are relatively higher. Previous studies reported that the (0 2 0) plane of $(VO)_2P_2O_7$ is acknowledged to be responsible for the catalytic activity in C_4 oxidation (Haber et al., 1997). The thickness of (2 0 4) face indicates the mean "length" at (2 0 4) face, while the actual thickness is represented by (0 2 0) plane (Esteman et al., 1995).

4.1.2 BET Surface Area Measurements and Chemical Analyses

As tabulated in Table 4.2, the specific surface area for VPS-6, VPS-18, VPS-30 and VPS-75 were 24.01 $m^2\ g^{-1}$, 19.38 $m^2\ g^{-1}$, 15.37 $m^2\ g^{-1}$ and 12.44 $m^2\ g^{-1}$, respectively. The specific surface area was found to be inversely proportional to the activation duration. This trend was in agreement with the results obtained from the XRD data, indicating that smaller crystallite size could exhibit higher specific surface area.

Table 4.2
Total surface area and average oxidation number of vanadium for bulk and Ba-doped VPS catalysts

Catalysts	Surface Area ($m^2 g^{-1}$)	P/V Ratio		Average Oxidation Number of Vanadium		
		EDX	ICP-OES	V^{5+} (%)	V^{4+} (%)	V_{av}
VPS-6	24	1.05	1.24	21	79	4.21
VPS-18	19	1.04	0.99	24	76	4.24
VPS-30	15	0.96	0.93	30	70	4.30
VPS-75	12	1.03	0.86	50	50	4.50
VPS-Ba-6	21	1.04	1.01	31	69	4.31
VPS-Ba-18	21	1.02	0.96	32	68	4.32
VPS-Ba-30	18	1.03	0.99	37	63	4.37
VPS-Ba-75	13	1.00	0.97	48	52	4.48

Calculation for Average Oxidation Number of Vanadium was showed in Appendix D.
Calculation for P/V Ratio for ICP-OES and EDX were showed in Appendix E and Appendix G, respectively.

The same trend was also observed for catalysts calcined in 0.75 % *n*-butane/air and prepared via the same sesquihydrate route (Taufiq-Yap et al., 2004). However, the trend was different for $(VO)_2P_2O_7$ catalyst obtained via organic method (Taufiq-Yap et al., 2001; Abon et al., 1995). Abon et al. reported that the increased of activation period would change the morphology of the catalysts particles and bring about the formation of more split $(VO)_2P_2O_7$, which increased the total surface area (Abon et al., 1995).

The catalysts calcined in 0.75 % *n*-butane/air via the same synthesis route gave higher crystallite size than the 1% O_2/N_2 activated counterparts (Taufiq-Yap et al., 2004). The catalysts prepared via organic route and activated under nitrogen atmospheres reported that lower surface area was obtained as compared to the VPS catalysts (Govender et al., 2004). Previous

studies reported that activation in a less oxidizing atmospheres such as CO_2 or inert atmosphere such as N_2 resulted in the formation of the crystalline $(VO)_2P_2O_7$ (Cheng and Wang, 1997).

As tabulated in Table 4.2, VPS Ba-6 and VPS Ba-18 had specific surface area of 21 m^2 g^{-1}. VPS Ba-30 and VPS Ba-75 had specific surface area of 18 m^2 g^{-1} and 13 m^2 g^{-1}, respectively. The specific surface area was found to be inversely proportional to activation duration. The same trend was observed for VPS Bulk catalysts prepared via the same route. The cation was incorporated into the vanadyl pyrophosphate in the solid solutions of type ($(VO)_{1-x}M_x)_2P_2O_7$) where M is a cation that substitutes for VO^{2+}, and the effect was only observed for relatively low concentrations of the promoter cation (Taufiq-Yap et al., 2003).

The total surface area obtained for Ba-doped catalysts are lower than that of VPS Bulk. Previous studies on the intercalation of alkaline metals (Li, Na, K, Rb, Cs) into vanadyl phosphate dihydrate reported that the intercalation was observed to cause a contraction in the interfoliar space owing to an electrostatic attraction between the vanadyl phosphate layers, which posses a negative charge due to vanadium (V) reduction, and the intercalating cation (Chauvel et al., 1995).

ICP-OES analysis revealed that bulk P/V atomic ratio (Table 4.2) of VPS-6, VPS-18, VPS-30 and VPS-75 was 1.24, 0.99, 0.93 and 0.86, respectively. This indicated that increased the activation duration decreased the

phosphorus content of the VPS catalysts. Previous studies reported that P/V ratio has high influence for the oxidation in of $(VO)_2P_2O_7$ to a V^{5+} phosphate during catalytic preparation (Cavani et al., 2000). As for the EDX analyses, results showed that P/V atomic ratio at the surface of VPS catalysts was in the range of 0.96-1.05. An enrichment of phosphorus at the surface was found on VPS-6 (P/V= 1.24). Previous studies reported that oxidation was facile at P/V ratio=0.9 whereas as the +4 oxidation state of vanadium was stabilized by excess phosphorus at P/V ratio greater than 1.0 (Hodnett and Delmon, 1984).

Bulk P/V atomic ratio obtained from ICP-OES analysis (Table 4.2) for VPS Ba-6, VPS Ba-18, VPS Ba-30 and VPS Ba-75 were 1.01, 0.96, 0.99 and 0.97, respectively. As for the EDX analyses, results showed that surface P/V atomic ratio of the VPS catalysts was in the range of 1.00-1.04. The enrichment of the phosphorus in VPO catalysts could help in stabilizing the reduced vanadium species and limit the over oxidation of the reduced vanadium species (Kalevaru et al., 2011; Guan et al., 2008). P/V atomic ration for Ba-doped VPS catalysts has no significant difference as compared to bulk VPS catalysts. Both the bulk and Ba-doped VPS catalysts have phosphorus content.

The average oxidation state of vanadium is directly proportional to the activation duration. Active and selective vanadium phosphate catalysts usually exhibit a mean oxidation state of vanadium slightly higher than 4.00 (Abon and Volta, 1997). The increment in the average oxidation state of vanadium was due to the presence of a V^{5+} phase. The percentage of V^{5+} increased from 21% for VPS-6 to 24 %, 30 % and 50 % for VPS-18, VPS-30 and VPS-75,

respectively (Table 4.2). However, the V^{4+} species appeared to be the major species as compared to the V^{5+} species.

The addition of 1 mol % Ba cation along with increasing activation duration yielded increasing average oxidation state of vanadium. The percentage of V^{4+} appeared to be the major species as compared to the V^{5+} phases, decreased from 69% for VPS Ba-6 to 68 %, 63 % and 52 % for VPS Ba-18, VPS Ba-30 and VPS Ba-75, respectively (Table 4.2). The average oxidation number of vanadium for Ba-doped VPS catalysts is slightly higher than that of VPS Bulk catalysts.

The Ba-doped VPS catalysts displayed slightly higher amount of V^{5+} as compared to that of VPS Bulk catalysts. This showed that the promoter affect the oxidizability of the VPO catalysts during activation. The result reflects that oxidized phases of $VOPO_4$ may exist in the catalysts structure of the Ba-doped VPS catalysts but could not be detected by XRD analysis.

The redox analyses for both the bulk and Ba-doped VPS catalysts are in agreement with the specific surface area analyses. The higher amount of reduced species (*i.e.* V^{4+} phase) in VPS catalyst activated at shorter duration (6 hours) yielded higher surface area. Catalysts with smaller surface area contains a mixture of $VOPO_4$ and $(VO)_2P_2O_7$ together with non-crystalline vanadium phosphates, whereas the large surface area catalyst contains more crystalline $(VO)_2P_2O_7$ (Rownaghi and Taufiq-Yap, 2009). As the composition of the V^{5+} increased, the abundance of the reduced species would correspondingly

decreased and the crystallization of V^{5+} occurred and resulted in a decrease in specific surface area (Cheng and Wang, 1997).

4.1.3 Scanning Electron Microscopy (SEM)

The surface morphologies of the bulk and Ba-doped VPS catalysts were showed in Figure 4.3 and Figure 4.4, respectively. Bulk and Ba-doped VPS catalysts consisted of plate-like crystals, which were agglomerated into different sizes of clusters. The structure of the crystal plates appeared to be very similar to the petals of rose flower, whereby certain edges of the crystal plates are folded. VPS catalysts prepared via the same synthetic route but calcined in 0.75 % *n*-butane/air had produced secondary structure, consisting different sizes of plate-like crystals with folded edges and were agglomerated into the characteristics of rosette-shape clusters (Taufiq-Yap et al., 2004).

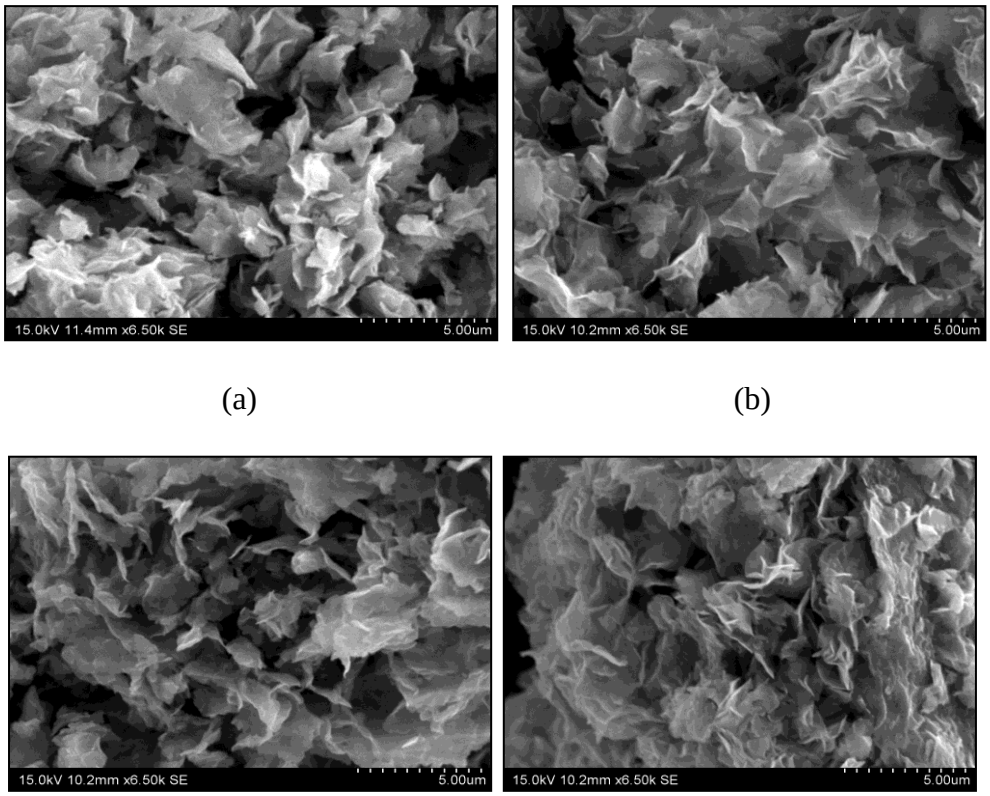

Figure 4.3: SEM micrographs of: (a) VPS-6; (b) VPS-18; (c) VPS-30; (d) VPS-75

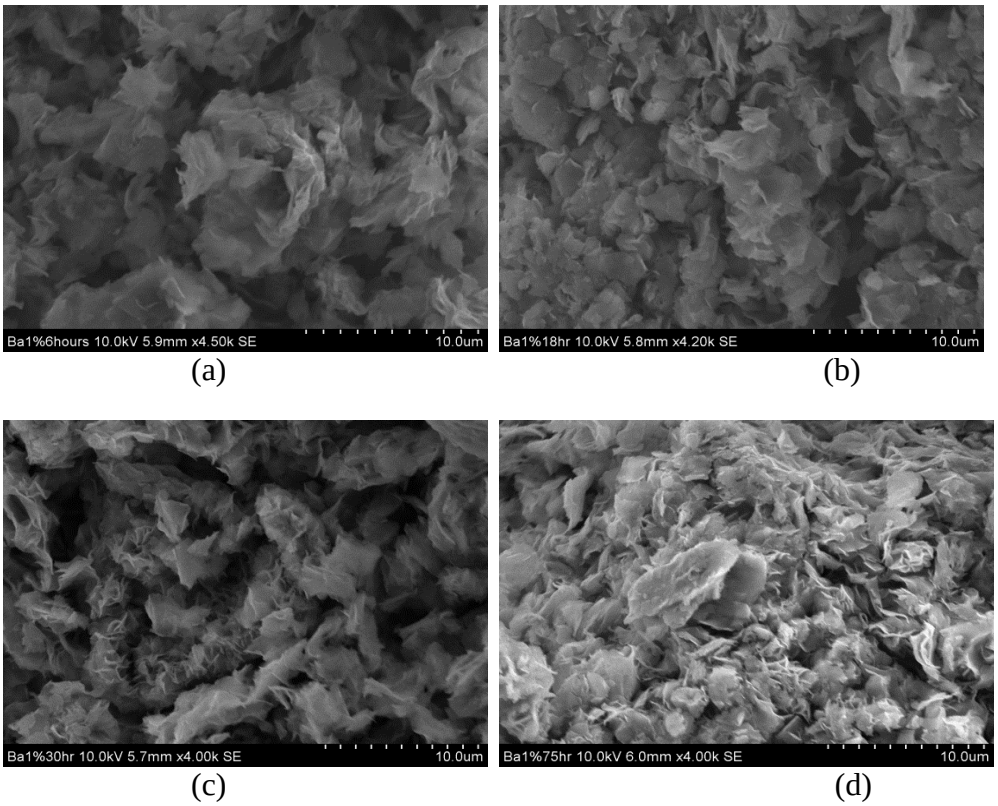

Figure 4.4: SEM micrographs of: (a) VPS Ba-6; (b) VPS Ba-18; (c) VPS Ba-30; (d) VPS Ba-75

Plate-like crystals with folded edge is an interesting feature possessed by VPS synthetic route, which differs from other well-known preparation methods, such as organic route, aqueous route, and reduction of $VOPO_4 \cdot 2H_2O$ (also known as VPO, VPA and VPD methods, respectively) (Taufiq-Yap et al., 2004).

As the activation duration increased from 6 to 75 hours, the amounts of larger plate-like crystals were found to increase as well. This indicated that some kind of sintering phenomenon occurred during the prolonged activation process, which led to a lower specific surface area.

VPS catalyst which had been activated for the longest period of time, *i.e.* 75 hours, appeared to have a more bulky structure when compared to the less activated counterparts. This may contribute to the decrease in the specific surface area of the longer activated counterparts. Previous studies had reported that VPO catalysts with higher amount of V^{4+} phase seems to have more splits and thus higher specific surface area was observed as compared to VPO catalysts with higher amount of V^{5+} (Abon et al., 1995).

4.1.4 Temperature-Programmed Desorption (TPD) of O_2

Figure 4.5 shows the TPD of O_2 profile for bulk VPS catalysts. The TPD of O_2 was carried out by pre-treating the sample to 673K in an oxygen flow (1 bar, 25cm^3 min^{-1}) and holding for 1 hour before cooling them to ambient temperature. The sample was then heated to 1173 K under helium flow (1 bar, 25cm^3 min^{-1}). Previous researchers had reported that, pretreatment carried out in purified oxygen at 673 K could remove all adsorbed water (Sakakini et al., 2000). TPD of O_2 profile showed that the desorption peak become more intense and shifted slightly to higher temperature as the activation duration increased from 6 to 75 hours.

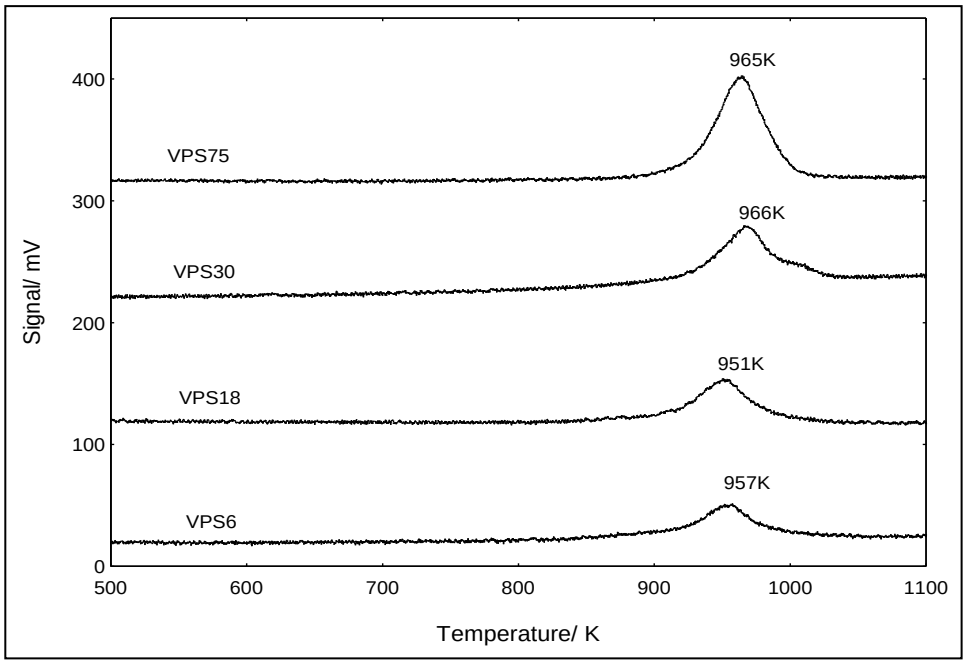

Figure 4.5: TPD of O_2 profiles for bulk VPS catalysts

The total amount of oxygen desorbed from the surface of the catalysts increased from 2.09 X 10^{20} atom g^{-1} for VPS-6 to 2.36 X 10^{20} atom g^{-1}, 3.46 X 10^{20} atom g^{-1} and 5.67 X 10^{20} atom g^{-1} for VPS-18, VPS-30 and VPS-75, respectively (Table 4.3). The peak was observed to be more prominent as the activation duration increased (Taufiq-Yap et al., 2004).

Table 4.3
Total amount of oxygen atoms desorbed, values of desorption activation energies obtained by temperature programmed desorption

Sample	Temperature Maxima, T_m (K)	Desorption Activation Energy, E_d (kJ mol^{-1})	Amount of Oxygen Desorbed (mol g^{-1})	Amount of Oxygen Desorbed (atom g^{-1})
VPS-6	957	264.27	3.47×10^{-4}	2.09×10^{20}
VPS-18	951	262.61	3.92×10^{-4}	2.36×10^{20}
VPS-30	966	266.76	5.74×10^{-4}	3.46×10^{20}
VPS-75	965	266.48	9.43×10^{-4}	5.67×10^{20}
VPS Ba-6	966	266.76	3.37×10^{-4}	2.03×10^{20}
VPS Ba-18	966	266.76	4.93×10^{-4}	2.97×10^{20}
VPS Ba-30	992	273.93	5.88×10^{-4}	3.54×10^{20}
VPS Ba-75	995	274.76	6.76×10^{-4}	4.07×10^{20}

Calculation for activation energy was showed in Appendix F.
Surface Area: VPS-6= 24 $m^2 g^{-1}$, VPS-18= 19 $m^2 g^{-1}$, VPS-30= 15 $m^2 g^{-1}$, VPS-75= 12 $m^2 g^{-1}$, VPS Ba-6= 21 $m^2 g^{-1}$, VPS Ba-18= 21 $m^2 g^{-1}$, VPS Ba-30= 18 $m^2 g^{-1}$, VPS Ba-75= 13 $m^2 g^{-1}$

The amount of oxygen atom desorbed from VPS-75 is about three times greater than the amount of oxygen desorbed from VPS-6. This has indicated that prolonged activation of sesquihydrate precursor in 1% O_2/N_2 favoured higher mobility of lattice oxygen. The trend was in agreement with the catalysts prepared via the same route and calcined in 0.75 % *n*-butane/ air. The only difference was that higher amount of oxygen atom could be desorbed from the VPS catalysts activated in 1% O_2/N_2 as compared to the previous study (Taufiq-Yap et al., 2004). However, this particular trend was in contrast to catalysts prepared via vanadyl phosphate dihydrate precursor and calcined in 0.75 % *n*-butane/ air, which reported that increasing activation duration could produce catalysts which desorbed less oxygen due to the role of the *n*-butane/ air pretreatment is to remove the unselective oxygen (Taufiq-Yap et al., 2001).

Figure 4.6 shows the TPD of O_2 profile for Ba-doped VPS catalysts. The desorption peak become more intense and shifted slightly to higher temperature as the activation duration increased. The total amount of oxygen desorbed from the surface of the catalysts increased from 2.03 X 10^{20} atom g^{-1} for VPS Ba-6 to 2.97 X 10^{20} atom g^{-1}, 3.54 X 10^{20} atom g^{-1} and 4.07 X 10^{20} atom g^{-1} for VPS Ba-18, VPS Ba-30 and VPS Ba-75, respectively (Table 4.3).

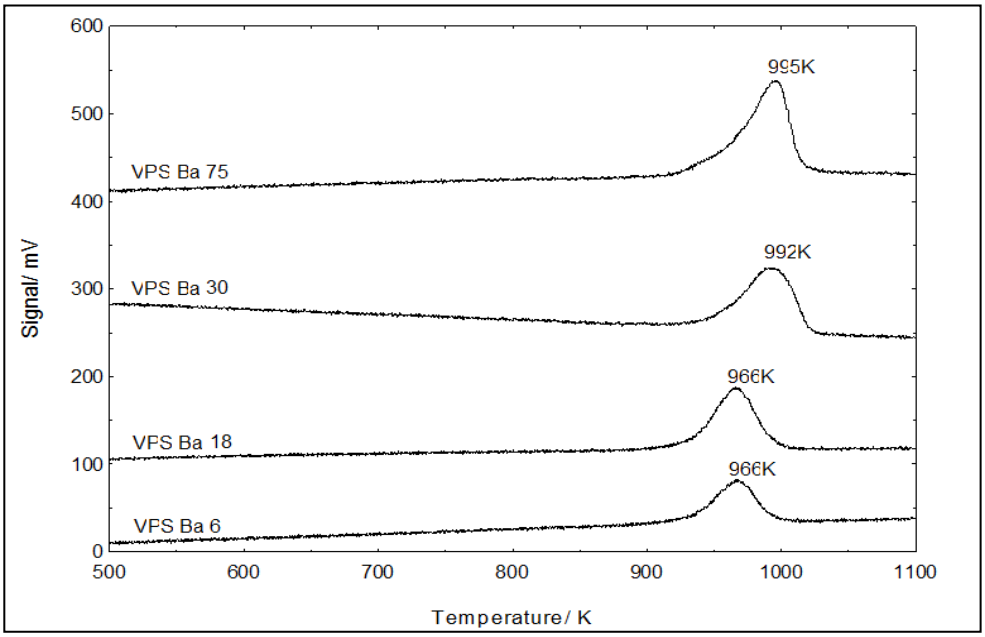

Figure 4.6: TPD of O_2 profiles for Ba-doped VPS catalysts

The amount of oxygen atom desorbed from VPS Ba-75 is about two times greater than the amount of oxygen desorbed from VPS Ba-6. This has indicated that prolonged activation of sesquihydrate precursor in 1% O_2/N_2 could favour higher mobility of lattice oxygen. This is same as that obtained for bulk VPS catalysts.

In general, the total amount of oxygen desorbed from the Ba-doped VPS catalysts is lower than that of bulk VPS catalysts. Higher maximum temperature is obtained for Ba-doped VPS catalysts as compared to VPS Bulk. Thus, relatively higher desorption activation energy is needed for Ba-doped VPS catalysts.

Desorption activation energies were obtained from Redhead equation as showed in equation 4.1:

$$\frac{E_d}{RT_m^2} = \left(\frac{A}{\beta}\right) \exp\left(\frac{-E_d}{RT_m}\right) \quad \text{..... (4.1)}$$

Where E_d is desorption activation energy (kJ mol^{-1}), *A* is desorption *A*-factor (10^{13} s^{-1}, assumed), R is the gas constant (J K^{-1} mol^{-1}), β is the heating rate (K s^{-1}) and T_m (K) is the temperature of the peak maximum (Redhead, 1962).

Desorption activation energy for VPS-6, VPS-18, VPS-30 and VPS-75 were 264.27 kJ mol^{-1}, 262.61 kJ mol^{-1}, 266.76 kJ mol^{-1} and 266.48 kJ mol^{-1}, respectively (Table 4.3). Bulk VPS catalysts with prolonged activation duration consumed greater amount of desorption energy as compared to the less activated counterparts. The desorption activation energy obtained was lower as compared to the catalysts prepared via the same synthetic route but calcined in 0.75 % *n*-butane/ air (Taufiq-Yap et al., 2004).

Desorption temperature for the 1 mol % Ba-doped VPS catalysts increased slightly as the activation duration increased, which has shown the increase in desorption activation energy. The desorption temperature VPS Ba-6

to VPS Ba-75 were in the range of 966-995K. This is slightly higher than that obtained for Bulk VPS-6 to VPS-75, which were in the range of 957-965K.

4.1.5 Temperature Programmed Reduction (TPR) in H_2

Figure 4.7 showed the TPR in H_2 profiles for bulk VPS catalysts. TPR in H_2 was obtained by heating the sample to 473 K in a purified nitrogen flow (25 cm^3 min^{-1}) and holding for 30 minutes before cooling to ambient temperature. The flow was then switched to 5 % H_2/N_2 (25 cm^3 min^{-1}) and the temperature was raised to 1173 K (5 K min^{-1}). The amount of oxygen atoms being removed, the peak maxima and the reduction activation energies for VPS catalysts were summarised in Table 4.4.

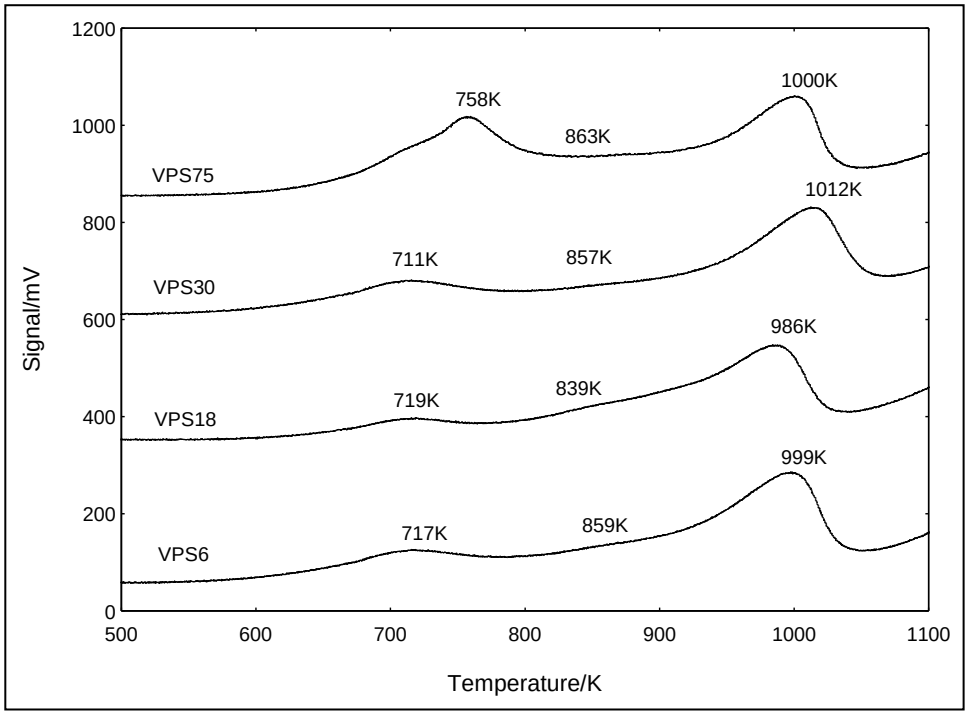

Figure 4.7: TPR in H_2 profile for bulk VPS Catalysts

Table 4.4
Total amount of oxygen atoms removed, values of reduction activation energies obtained by temperature programmed reduction

Sample	Temperature Maxima, T_m (K)	Reduction Activation Energy, E_r (kJ mol^{-1})	Amount of Oxygen Removed (mol g^{-1})	Amount of Oxygen Removed (atom g^{-1})
VPS6	717	119.70	5.37 $X10^{-4}$	3.23 $X10^{20}$
	859	143.40	4.72 $X10^{-4}$	2.84 $X10^{20}$
	999	166.77	1.61 $X10^{-3}$	9.69 $X10^{20}$
Total			**2.62 $X10^{-3}$**	**1.58 $X10^{21}$**
VPS18	719	120.03	3.89 $X10^{-4}$	2.34 $X10^{20}$
	839	140.06	6.52 $X10^{-4}$	3.93 $X10^{20}$
	986	164.60	1.62 $X10^{-3}$	9.75 $X10^{20}$
Total			**2.66 $X10^{-3}$**	**1.60 $X10^{21}$**
VPS30	711	118.70	7.48 $X10^{-4}$	4.50 $X10^{20}$
	857	143.07	3.89 $X10^{-4}$	2.34 $X10^{20}$
	1012	168.94	1.81 $X10^{-3}$	1.09 $X10^{21}$
Total			**2.95 X 10^{-3}**	**1.78 $X10^{21}$**
VPS75	758	126.54	1.75 $X10^{-3}$	1.05 $X10^{21}$
	863	144.07	5.74 $X10^{-4}$	3.45 $X10^{20}$
	1000	166.94	1.94 $X10^{-3}$	1.17 $X10^{21}$
Total			**4.26 $X10^{-3}$**	**2.57 $X10^{21}$**
VPS Ba-6	735	122.70	6.93 $X10^{-4}$	4.17 $X10^{20}$
	1019	170.11	1.38 $X10^{-3}$	8.29 $X10^{20}$
Total			**2.07 $X10^{-3}$**	**1.25 $X10^{21}$**
VPSBa-18	752	125.54	1.11 $X10^{-3}$	6.66 $X10^{20}$
	1031	172.12	1.31 $X10^{-3}$	7.89 $X10^{20}$
Total			**2.42 $X10^{-3}$**	**1.46 $X10^{21}$**
VPS Ba-30	857	143.07	1.41 $X10^{-3}$	8.48 $X10^{20}$
	1076	179.63	1.70 $X10^{-3}$	1.02 $X10^{21}$
Total			**3.11 X 10^{-3}**	**1.87 $X10^{21}$**
VPS Ba-75	844	140.90	2.46 $X10^{-3}$	1.48 $X10^{21}$
	1046	174.62	1.38 $X10^{-3}$	8.31 $X10^{20}$
Total			**3.84 $X10^{-3}$**	**2.31 $X10^{21}$**

Calculation for activation energy was showed in Appendix F.

Three peak maxima were observed. The first and second peaks corresponded to the reduction of V^{5+} phase, while the third peak was corresponded to the reduction of V^{4+} phase (Taufiq-Yap et al., 2004). The peak attributed to V^{4+} associated with the removal of O^- anion while the peak attributed to the removal of O^{2-} anion associated with the V^{5+} phase (Abon and Herrmann, 2001). The reduction of V^{4+} appeared to be the major peak and this indicated that V^{4+} is the predominant species in the catalyst, as shown by the results obtained from redox and XRD.

As tabulated in Table 4.4, the VPS-6 catalyst gave three peaks maxima at temperature of 717 K, 859 K and 999 K with the amount of oxygen removed in each peak was 3.23 $X10^{20}$, 2.84 $X10^{20}$ and 9.69 $X10^{20}$ atom g^{-1}, respectively. VPS-18 showed three reduction peaks appeared at 719 K, 839 K and 986 K with the amount of oxygen removed were 2.34 X 10^{20} mol g^{-1}, 3.93 X 10^{20} mol g^{-1} and 9.75 X 10^{20} mol g^{-1}, respectively. As for the VPS-30, three reduction peaks were observed at 711 K, 857 K and 1012 K with the amount of oxygen removed were 4.50 X 10^{20} mol g^{-1}, 2.34 X 10^{20} mol g^{-1} and 1.09 X 10^{21} mol g^{-1}, respectively. VPS 75 showed three reduction peaks observed at 758 K, 863 K and 1000 K with the amount of oxygen being removed were 1.05 X 10^{21} mol g^{-1}, 3.45 X 10^{20} mol g^{-1} and 1.17 X 10^{21} mol g^{-1}, respectively.

Increasing the activation duration could induce greater amount of oxygen species removed from the catalysts. This showed an increased reactivity and mobility of lattice oxygen (Taufiq-Yap and Saw, 2008). This trend was similar to the sesquihydrate precursor calcined in *n*-butane/air

environment (Taufiq-Yap et al., 2004). Increasing the activation duration in 1% O_2/N_2 shifted all the three reduction peaks to higher temperature.

Figure 4.8 shows the TPR in H_2 profiles for Ba-doped VPS catalysts. The amount of oxygen atoms being removed, the peak maxima and the reduction activation energies for VPS catalysts were summarized in Table 4.4.

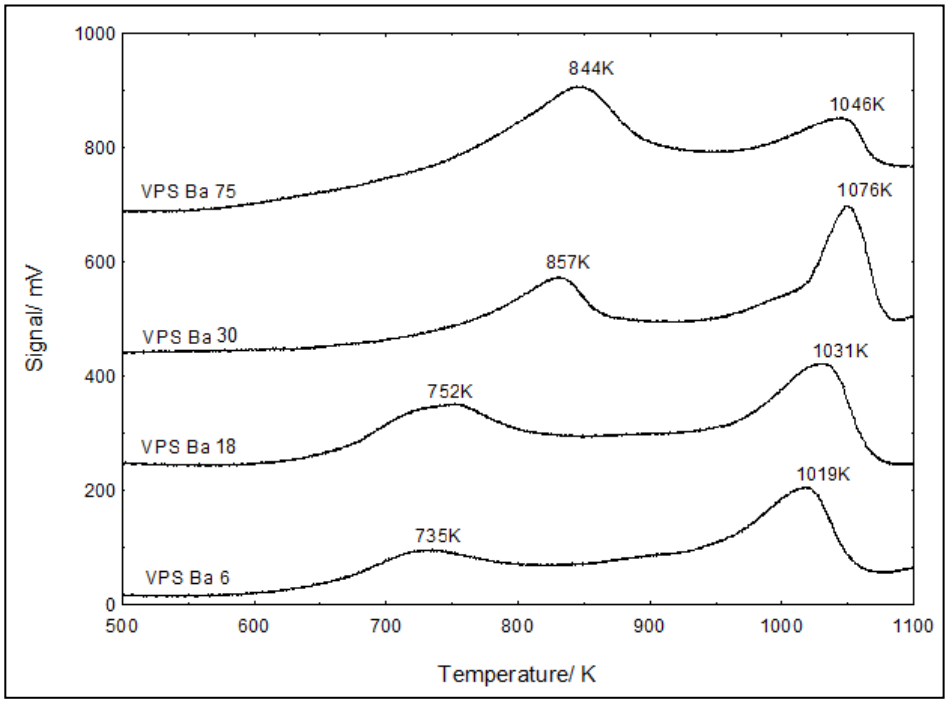

Figure 4.8: TPR in H_2 profile for Ba-doped VPS catalysts

Two peak maxima were observed. The first peak corresponded to the reduction of V^{5+} phase, whereas the second peak is assigned to the removal of lattice oxygen from the active V^{4+} phase (Taufiq-Yap et al., 2004). The peak attributed to V^{4+} is associated to the removal of O^- anion while the peak attributed to the removal of O^{2-} anion associated to the V^{5+} phase (Volta, 2000; Goh et al., 2008). The first peak shifted to the right as the activation duration

increased, indicating that the reduction temperature increased as the activation duration increased.

The reduction of V^{4+} appeared to be the major peak for VPS Ba-6, VPS Ba-18 and VPS Ba-30 and this indicated that V^{4+} is the predominant species in the catalyst, as evidenced by the results obtained from redox and XRD. As for the VPS Ba-75, the reduction peak of V^{5+} phase appeared to be the major peak. This increases the crystallite size and reduces the specific surface area of the Ba-doped VPS catalysts.

As tabulated in Table 4.4, VPS Ba-6 catalyst gave two peak maxima in the rate of hydrogen consumption at 735 K and 1019 K with the amount of oxygen atoms removed for each peak was 4.17 X 10^{20} and 8.29 X 10^{20} atom g^{-1}, respectively. VPS Ba-18 showed two reduction peaks appeared at 752 K and 1031 K with the amount of oxygen removed were 6.68 X 10^{20} mol g^{-1} and 6.68 X 10^{20} mol g^{-1}, respectively. As for the VPS Ba-30, two reduction peaks were observed at 857 K and 1076 K with the amount of oxygen removed were 8.48 X 10^{20} mol g^{-1} and 1.00 X 10^{21} mol g^{-1}, respectively. As for the VPS-75, the two reduction peaks were observed at 844 K and 1046 K with the amount of oxygen being removed were 1.48 X 10^{21} mol g^{-1} and 8.31 X 10^{20} mol g^{-1}, respectively.

4.1.6 Selective oxidation of *n*-butane to Maleic Anhydride

The details of the catalytic performance data for VPS catalysts were shown in Table 4.5. VPS-6, VPS-18, VPS-30 and VPS-75 exhibited *n*-butane conversion of 14 %, 14 %, 10 % and 7 %, respectively. The main by-products were CO and CO_2.The *n*-butane conversion decreased as the activation duration increased to 75 hours due to the higher amount of V^{5+} found as shown in XRD. Previous research proposed that $VOPO_4$ phases would be detrimental but small number of V^{5+} species would be required for the oxygen insertion into the hydrocarbon intermediates according to a redox reaction (Abon et al., 1995). However, all the catalysts revealed high selectivity, *i.e.* 90 % and above. The MA selectivity obtained for VPS-6, VPS-18, VPS-30 and VPS-75 were in the range of 90-93%. These showed that selectivity of MA was not markedly affected by the activation duration.

Table 4.5
Catalytic performance of bulk and Ba-doped VPS catalysts

Catalysts	*n*-butane conversion (%)	Product Selectivity (%)		
		MA	CO	CO_2
VPS-6	14	93	5	2
VPS-18	14	94	5	2
VPS-30	10	90	8	2
VPS-75	7	91	7	2
VPS Ba-6	17	94	5	1
VPS Ba-18	12	93	5	2
VPS Ba-30	13	91	7	2
VPS Ba-75	6	90	7	3

Surface Area: VPS-6= 24 $m^2 g^{-1}$, VPS-18= 19 $m^2 g^{-1}$, VPS-30= 15 $m^2 g^{-1}$, VPS-75= 12 $m^2 g^{-1}$, VPS Ba-6= 21 $m^2 g^{-1}$, VPS Ba-18= 21 $m^2 g^{-1}$, VPS Ba-30= 18 $m^2 g^{-1}$, VPS Ba-75= 13 $m^2 g^{-1}$

The details of the catalytic performance data for Ba-doped VPS catalysts activated in 1% O_2/N_2 were shown in Table 4.5. VPS Ba-6, VPS Ba-18, VPS Ba-30 and VPS Ba-75 showed *n*-butane conversion of 17 %, 12 %, 13 % and 6 %, respectively. The decreasing trend of the catalytic activity of the Ba-doped VPS catalysts was due to the decreasing BET surface area corresponding to the development of (0 2 0) plane of $(VO)_2P_2O_7$. There is a linear relationship between *n*-butane conversions and catalysts surface area (Taufiq-Yap et al., 2003; Hutchings and Higgins, 1996). Previous studies reported that the low surface area of each sample, which is inherited from that of the precursor, limits strongly the butane conversion (Duvauchelle and Bordes, 1999).

The MA selectivity of Ba-doped VPS catalysts was only slightly affected by increasing activation duration. The MA selectivity obtained for VPS Ba-6, VPS Ba-18, VPS Ba-30 and VPS Ba-75 were in the range of 90-94%. The yield in MA decreased as activation duration increased from 6 hours to 18 hours, 30 hours and 75 hours. A synergetic effect of a well-dispersed nanocrystalline V^{5+} phase in the major well crystalline pyrophosphate phase led to the enhancement of the *n*-butane activation and the production of MA (Rownaghi and Taufiq-Yap, 2009).

The *n*-butane conversion for VPS Bulk catalysts are slightly lower than that of Ba-doped VPS catalysts, which is in the range of 7-14%. However, the maleic anhydride selectivity for VPS Bulk is similar to that of Ba-doepd VPS catalysts, which is in the range of 90-93%.

4.2 Effect of Mg, Ca and Sr-doped VPS Catalysts

The effect of activation duration for bulk and Ba-doped VPS catalysts was examined. The optimum activation duration was selected and proceeded with the study of the effect on Mg, Ca and Sr doped VPS catalysts.

4.2.1 X-Ray Diffraction (XRD)

The XRD pattern of the 3 mol % alkaline earth metal-doped VPS catalysts activated at 733 K in a reaction flow of 1% O_2/N_2 for 6 hours was shown in Fig. 4.9. The diffractogram showed that VPS-Mg, VPS-Ca and VPS-Sr catalysts comprised of similar diffraction pattern of well-crystallized $(VO)_2P_2O_7$ phase with three main characteristic peaks appeared at 2θ= 22.9°, 28.4° and 29.8° (JCPDS File No. 34-1381), which corresponding to the reflection planes of (0 2 0), (2 0 4) and (2 2 1), respectively.

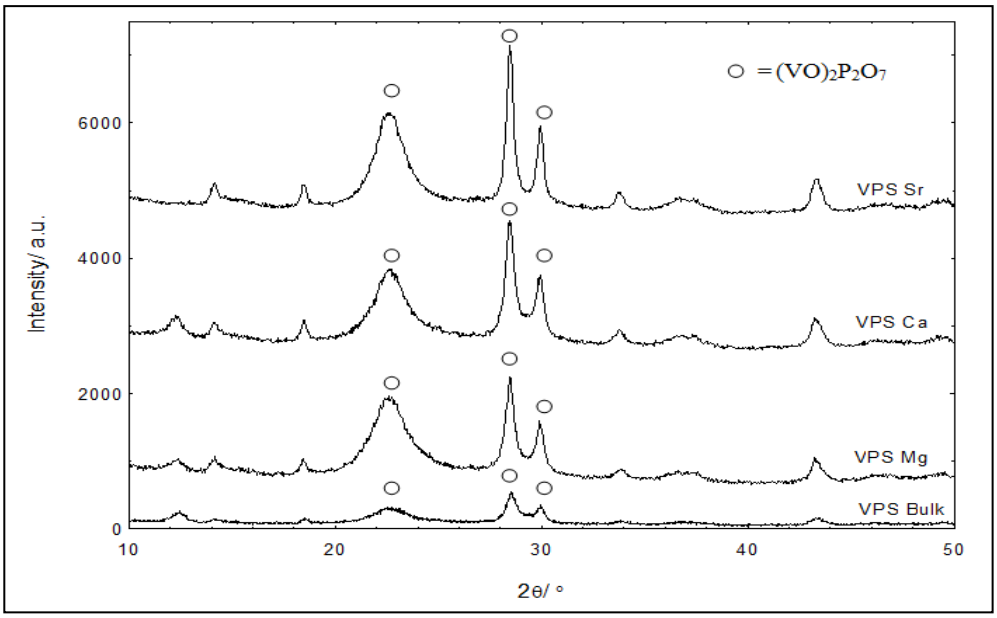

Figure 4.9: Powdered XRD patterns of bulk and alkaline earth metal-doped VPS catalysts

The addition of alkaline earth metals from Mg to Sr has led to the increasing intensity of the three major peaks at 2θ = 22.9°, 28.4° and 29.8°. This indicated that the addition of alkaline-earth metals from Mg to Sr in VPS catalysts could enhance the formation of V^{4+} phase. Previous studies reported that all alkali and alkali-earth metal doped VPO catalysts produced via organic method contained $(VO)_2P_2O_7$ phase without any exception (Zazhigalov et al., 1996).

There is a trend of decreasing crystallite size from VPS-Mg to VPS-Ca and VPS-Sr. The crystallite sizes of the (0 2 0) reflection plane for VPS-Mg, VPS-Ca and VPS-Sr were calculated as 47.66 Å, 45.35 Å and 41.17 Å, respectively, whereas the crystallite sizes of (2 0 4) reflection plane for the same series of catalysts were calculated as 119.62 Å, 113.94 Å and 105.76 Å, respectively (Table 4.6). This indicates that the addition of alkaline earth

metals from Mg to Sr led to the increased in the specific surface area of the VPS catalysts. This is supported by the result obtained from BET analyses.

Table 4.6
XRD data for the bulk and alkaline-earth metal-doped VPS catalysts

Catalysts	Line width [a] (020) (°)	Line width [b] (204) (°)	Crystallite Size [c] (020) (Å)	Crystallite Size [c] (204) (Å)
VPS bulk	2.1000	0.6889	38.12	117.56
VPS-Mg	1.6805	0.6769	47.66	119.62
VPS-Ca	1.7656	0.7108	45.35	113.94
VPS-Sr	1.9449	0.7657	41.17	105.76

Calculation for crystallite size was showed in Appendix C.
[a] FWHM of (020) reflection
[b] FWHM of (204) reflection
[c] Crystallite thickness by means of Scherrer's formula

The bulk VPS catalyst has the lowest crystallite size as compared to the alkaline-earth metal doped VPS catalysts. The parameter used to determine the crystallite size is the half width of the (0 2 0) peak. The line width decreased with increasing crystallite size. The decrease in the FWHM of the (0 2 0) reflection indicates that the thickness of the particles in the (1 0 0) directions decreases (Taufiq-Yap et al., 2006).

The addition of alkaline earth metal (Mg, Ca and Sr) into the VPS catalysts have shown to produce catalysts with larger crystallite size in the (0 2 0) direction as compared to the VPS Bulk. This indicates that the addition of the alkaline-earth metal into VPS catalysts would generally decrease the specific surface area of the catalysts.

4.2.2 BET Surface Area Measurements and Chemical Analyses

The specific surface area (Table 4.7) for VPS-Mg, VPS-Ca and VPS-Sr were 11 m^2 g^{-1}, 13 m^2 g^{-1} and 20 m^2 g^{-1}, respectively. There is a trend of increasing specific surface area from VPS-Mg to VPS-Sr. This is in agreement with the XRD results, indicating that smaller crystallite size would generally give higher specific surface area. The addition of the alkaline earth metal into VPS catalysts has shown to produce lower specific surface area as compared to the bulk VPS catalyst. The specific surface area obtained for alkali-earth metal doped-VPS catalysts is lower as compared to previous studies. Zazhigalov et al. (1996) reported that the introduction of the alkaline and alkaline earth metals did not change the specific surface area of the VPO catalysts prepared via organic method. The observed specific surface area for VPO catalysts scattered around the mean value of 29 m^2 g^{-1} (Zazhigalov et al., 1996).

Table 4.7
Total surface area and average oxidation number of vanadium for bulk and alkaline-earth metal-doped VPS catalysts

Catalysts	Specific Surface Area (m^2 g^{-1})	EDX	ICP-OES	Average Oxidation Number of Vanadium		
			P/V Ratio	V^{5+} (%)	V^{4+} (%)	V_{av}
VPS Bulk	24	1.05	1.24	21	79	4.21
VPS-Mg	11	1.07	0.94	31	69	4.31
VPS-Ca	13	1.08	0.97	24	76	4.24
VPS-Sr	20	1.04	0.93	23	77	4.23

Calculation for Average Oxidation Number of Vanadium was showed in Appendix D.
Calculation for P/V Ratio for ICP-OES and EDX were showed in Appendix E and Appendix G, respectively.

ICP-OES analysis revealed that the P/V atomic ratio (Table 4.7) obtained for VPS-Mg, VPS-Ca and VPS-Sr were 0.94, 0.97 and 0.93, respectively. EDX analyses revealed that P/V atomic ratio is in the range of 1.04- 1.08. The incorporation of alkaline-earth metal into VPS catalysts lower the phosphorus surface enrichment of the catalysts due to the decrease in the P/V ratio. However, Zazhigalov et al. (1996) reported that introduction of alkali and alkali-earth metals to the VPO catalysts causes an increase of surface P/V ratio as supported by the result obtained from XPS and XMPA showing that the enrichment of surface with phosphorus occurs at the expense of outward diffusion of over-stoichiometric phosphorus through the pellet.

The average oxidation states (Table 4.7) for VPS-Mg, VPS-Ca and VPS-Sr are 4.31, 4.24 and 4.23, respectively. Average oxidation states of vanadium for alkaline earth metals-doped VPS catalysts are higher than that of VPS Bulk. The percentage of V^{4+} appeared to be the major species as compared to the V^{5+} phases. The percentage of V^{4+} increased from 69 % for VPS-Mg to 76 % for VPS-Ca and 77 % for VPS-Sr. This is in agreement with the surface area results indicated that VPS catalysts with higher amount of V^{4+} could exhibit higher specific surface area.

4.2.3 Scanning Electron Microscopy (SEM)

The surface morphology of the alkaline earth metal-doped VPS catalysts is shown in Figure 4.10. The alkaline-earth metal-doped VPS catalysts consisted of plate-like crystals, which are arranged into the

characteristics rosette-shape clusters. Based on earlier works, the rosette-type agglomerates were made up of $(VO)_2P_2O_7$ platelets that preferentially expose the (020) crystal planes (Taufiq-Yap and Saw, 2008).

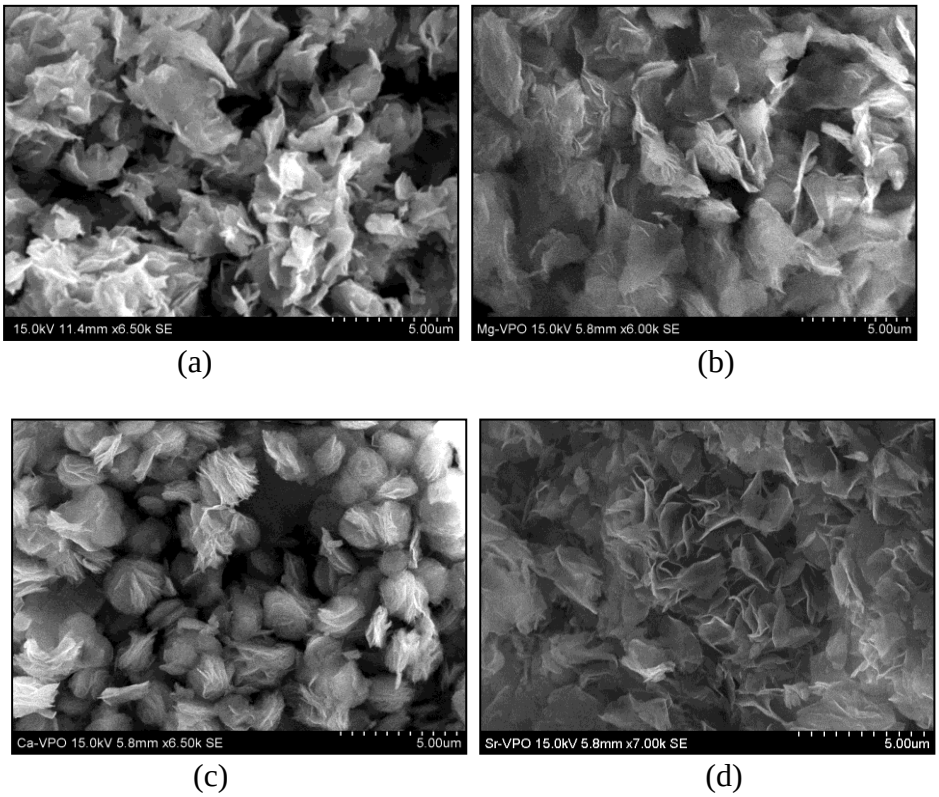

Figure 4.10: SEM micrographs of: (a) VPS Bulk; (b) VPS-Mg; (c) VPS-Ca; (d) VPS-Sr

The plate-like crystals obtained for VPS-Sr was found to have more splits as compared to VPS-Mg and VPS-Ca. This may contribute to the increase in specific surface area. Some of the edges of the crystal plates are found to be folded. This interesting feature was seen in catalysts prepared via vanadyl hydrogen sesquihydrate route and calcined in 0.75% *n*-butane/air. However, this feature was not found in catalysts prepared via other well-known methods, such as organic route or dihydrate route (Taufiq-Yap et al., 2004).

4.2.4 Temperature-Programmed Desorption (TPD) of O_2

Figure 4.11 shows the TPD of O_2 Profile for undoped and doped VPS catalysts. The analyses was carried out by pre-treating the sample to 673K in an oxygen flow (1 bar, 25 cm^3 min^{-1}) and holding for 1 hour before cooling them to ambient temperature. The sample was then heated to 1173 K under helium flow (1 bar, 25 cm^3 min^{-1}).

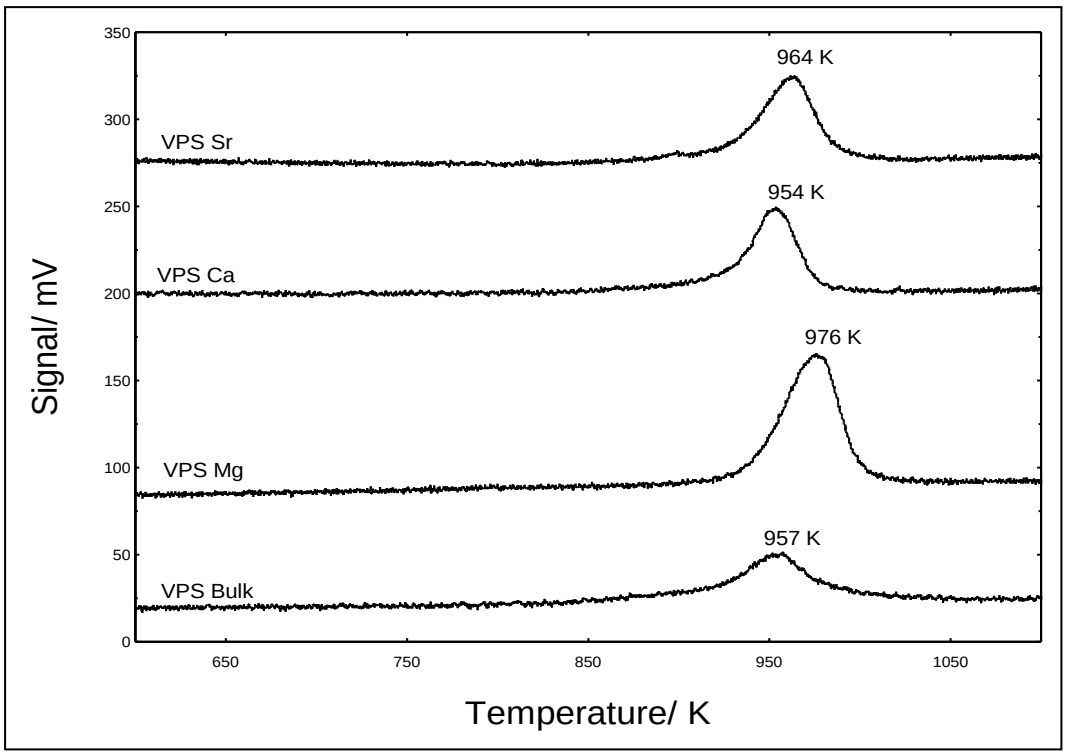

Figure 4.11: TPD of O_2 profile for VPS bulk, VPS-Mg, VPS-Ca and VPS-Sr catalysts

TPD of O_2 profile shows that the intensity of the alkaline earth metal doped VPS catalysts are higher than that of VPS Bulk. The intensity for VPS-Mg was found to be the highest as compared to that of VPS-Ca and VPS-Sr. There is a decreasing trend of the amount of oxygen desorbed from the VPS-Mg to VPS-Sr. As tabulated in Table 4.8, the amount of oxygen desorbed from

VPS-Mg, VPS-Ca and VPS-Sr are 3.12 X 10^{20} atom g^{-1}, 1.84 X 10^{20} atom g^{-1} and 1.67 X 10^{20} atom g^{-1}, respectively. This indicates that the mobility of surface oxygen is greater for VPS-Mg as compared to that of VPS-Ca and VPS-Sr. The amount of oxygen desorbed from VPS bulk is 2.086 X 10^{20} atom g^{-1}, which is greater than that of VPS-Ca and VPS-Sr but less than that obtained for VPS-Mg.

Table 4.8
Total amount of oxygen atoms desorbed, values of desorption activation energies obtained by temperature programmed desorption

Sample	Temperature Maxima, T_m (K)	Desorption Activation Energy, E_d (kJ mol^{-1})	Amount of Oxygen Desorbed (mol g^{-1})	Amount of Oxygen Desorbed (atom g^{-1})
VPS Bulk	957	264.27	3.47 X 10^{-4}	2.09 X 10^{20}
VPS-Mg	976	269.52	5.18 X 10^{-4}	3.12 X 10^{20}
VPS-Ca	954	263.44	3.06 X 10^{-4}	1.84 X 10^{20}
VPS-Sr	964	266.20	2.78 X 10^{-4}	1.67 X 10^{20}

Calculation for activation energy was showed in Appendix F.
Surface Area: VPS Mg= 11 m^2 g^{-1}, VPS Ca= 13 m^2 g^{-1}, VPS Sr= 20 m^2 g^{-1}

The desorption temperature for VPS-Mg, VPS-Ca and VPS-Sr are in the range of 954-976 K. Desorption activation energy for alkaline earth metal-doped VPS Catalysts are in the range of 263.44 - 269.52 kJ mol^{-1} while the desorption activation energy for VPS Bulk was 264.27 kJ mol^{-1}. This indicated that the desorption activation energy was not markedly affected by the addition of dopant. Higher activation energy indicates that the oxygen molecules bonded stronger on the surface of the VPS catalysts (Chorkendorff and Niemantsverdriet, 2003).

4.2.5 Temperature Programmed Reduction (TPR) in H_2

Figure 4.12 shows the TPR in H_2 profile for bulk and doped VPS catalysts. TPR in H_2 was obtained by heating the sample to 473 K in a purified nitrogen flow (25 cm^3 min^{-1}) and holding for 30 minutes before cooling to ambient temperature. The flow was then switched to 5 % H_2/N_2 (25 cm^3 min^{-1}) and the temperature was raised to 1173 K (5 K min^{-1}).

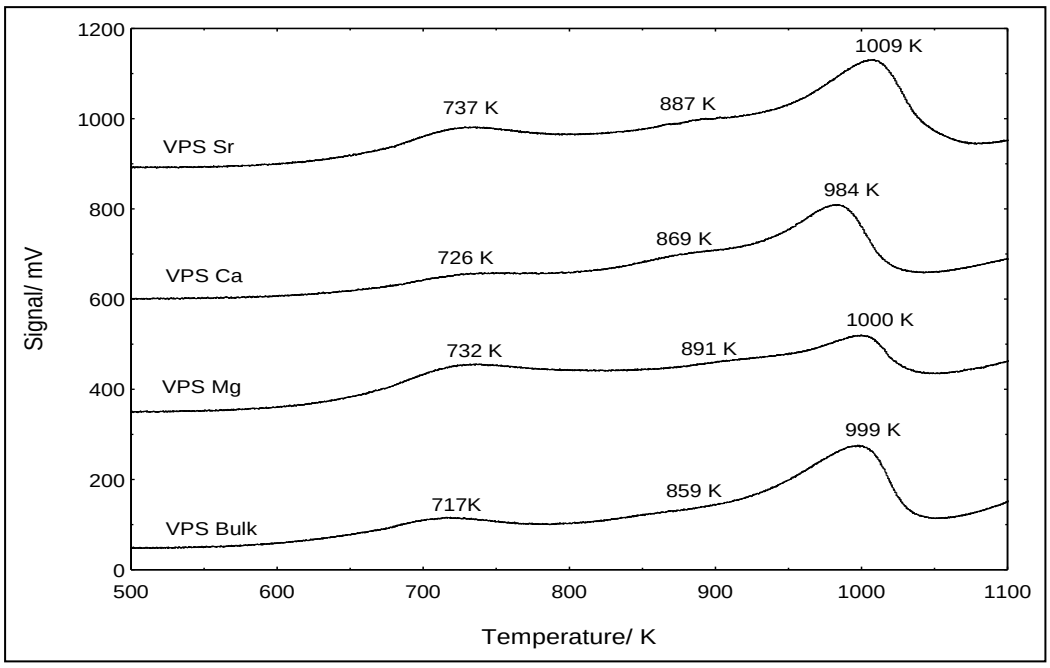

Figure 4.12: TPR in H_2 profile for bulk and alkaline earth metal-doped VPS catalysts

Three peaks maxima were observed. The first and second peaks corresponded to the reduction of V^{5+} phase while the third peak was corresponded to the reduction of V^{4+} phase. The peak attributed to V^{4+} associated to the removal of O^- anion while the peak attributed to V^{5+} associated to the removal of O^{2-} anion (Taufiq-Yap et al., 2004). The reduction

of V^{4+} appears to be the major peak and this indicated that V^{4+} is the predominant species in the catalyst, as shown by the result from redox reaction.

Total amount of oxygen removed from VPS-Mg, VPS-Ca and VPS-Sr were 1.47 $X10^{21}$ atom g^{-1}, 1.55 $X10^{21}$ atom g^{-1} and 1.90 $X10^{21}$ atom g^{-1}, respectively (Table 4.9). The addition of alkaline-earth metal from Mg to Sr induce greater amount of oxygen species removed from the catalysts, which had shown an increased reactivity and mobility of lattice oxygen (Taufiq-Yap and Saw, 2008). Total amount of oxygen removed from VPS Bulk was 1.58 $X10^{21}$ atom g^{-1}. VPS-Sr induce greater amount of oxygen species being removed, as compared to VPS Bulk. However, VPS-Mg and VPS-Ca have lower amount of oxygen species being removed from the catalysts, as compared to VPS Bulk.

VPS-Mg gave three peak maxima in the rate of hydrogen consumption at 732 K, 891 K and 1000 K with the amount of oxygen atoms removed for each peak was 6.71 $X10^{20}$ atom g^{-1}, 2.64 $X10^{20}$ atom g^{-1} and 5.38 $X10^{20}$ atom g^{-1}, respectively. VPS-Ca showed three reduction peaks appeared at 726 K, 869 K and 984 K with the amount of oxygen removed were 3.96 $X10^{20}$ atom g^{-1}, 3.66 $X10^{20}$ atom g^{-1} and 7.85 $X10^{20}$ atom g^{-1}, respectively. VPS-Sr gave three reduction peaks appeared at 737 K, 887 K and 1009 K with the amount of oxygen removed were 4.72 $X10^{20}$ atom g^{-1}, 3.18 $X10^{20}$ atom g^{-1} and 1.11 $X10^{20}$ atom g^{-1}, respectively. This indicated that the reactivity and mobility of the lattice oxygen increased as the basicity of the dopant increased from Mg to Sr.

Table 4.9
Total amount of oxygen atoms removed, values of reduction activation energies obtained by temperature programmed reduction

Sample	Temperature Maxima, Tm (K)	Reduction Activation Energy, E_r (kJ mol^{-1})	Amount of Oxygen Removed (mol/g)	Amount of Oxygen Removed (atom/g)
VPS Bulk	717	119.70	$5.37 X10^{-4}$	$3.23 X10^{20}$
	859	143.40	$4.72 X10^{-4}$	$2.84 X10^{20}$
	999	166.77	$1.61 X10^{-3}$	$9.69 X10^{20}$
Total				**$1.58 X10^{21}$**
VPS-Mg	732	122.20	$1.115 X10^{-3}$	$6.71 X10^{20}$
	891	145.39	$4.386 X10^{-4}$	$2.64 X10^{20}$
	1000	166.94	$8.930 X10^{-4}$	$5.38 X10^{20}$
Total				**$1.47 X10^{21}$**
VPS-Ca	726	121.20	$6.569 X10^{-4}$	$3.96 X10^{20}$
	869	145.07	$6.073 X10^{-4}$	$3.66 X10^{20}$
	984	164.27	$1.304 X10^{-3}$	$7.85 X10^{20}$
Total				**$1.55 X10^{21}$**
VPS-Sr	737	123.04	$7.838 X10^{-4}$	$4.72 X10^{20}$
	887	148.08	$5.278 X10^{-4}$	$3.18 X10^{20}$
	1009	168.44	$1.844 X10^{-3}$	$1.11 X10^{21}$
Total				**$1.90 X10^{21}$**

Calculation for activation energy was showed in Appendix F.

4.2.6 Selective oxidation of *n*-butane to Maleic Anhydride

The details of the catalytic performance data for doped and undoped VPS catalysts are shown in Table 4.10. The *n*-butane conversion for VPS-Mg, VPS-Ca and VPS-Sr are 10%, 13% and 17%, respectively. The *n*-butane conversation for VPS-Mg and VPS-Ca are slightly lower than that of VPS Bulk but VPS-Sr showed higher *n*-butane conversation than VPS Bulk. There is a trend of increasing *n*-butane conversion from VPS-Mg to VPS-Sr owing to their higher specific surface area as analyzed by BET measurements. Zazhigalov et al (1996) reported that addition of alkali and alkali-earth elements to VPO composition allow changing both activity and selectivity of the catalysts. Previous studies reported that the principal role of the promoter is

to enable the formation of high surface area catalysts corresponding to the development of (0 2 0) plane of $(VO)_2P_2O_7$ (Rownaghi and Taufiq-Yap, 2009).

Table 4.10
Catalytic performance of bulk and alkaline earth metal-doped VPS catalysts

Catalysts	*n*-butane conversion (%)	Product Selectivity (%)		
		MA	CO	CO_2
VPS Bulk	14	93	5	2
VPS-Mg	10	89	8	3
VPS-Ca	13	90	7	3
VPS-Sr	17	93	5	2

Surface Area: VPS Bulk= 24 $m^2 g^{-1}$, VPS Mg= 11 $m^2 g^{-1}$, VPS Ca= 13 $m^2 g^{-1}$, VPS Sr= 20 $m^2 g^{-1}$

The MA selectivity obtained for VPS-Mg, VPS-Ca and VPS-Sr were in the range of 89-93%. The MA selectivity was not markedly affected by the addition of dopants but there is a trend of increasing MA selectivity from VPS-Mg to VPS-Sr. Previous studies reported that a trend of increasing selectivity of MA formation when going from magnesium to barium, due to the increasing natural basicity of the added modifier (Brutovský et al., 1996).

Chapter 7

Conclusions

Bulk and alkaline earth metal-doped VPS catalysts were synthesized successfully via vanadyl hydrogen phosphate sesquihydrate route and activated in 1% O_2/N_2. The first part of the research involved the study of the effect of activation duration for bulk and Ba-doped VPS catalysts. The second part involved the study of the effect of Mg, Ca, and Sr-doped VPS catalysts.

Bulk and Ba-doped VPS catalysts showed that shorter activation duration yielded higher *n*-butane conversion. This catalytic result is in agreement with the result from physical, chemical and reactivity analyses.

XRD analysis revealed that increasing activation duration for bulk VPS catalysts would enhance the formation of V^{5+} phase. This may be due to the over oxidation of the VPS catalysts at longer activation duration. As for the Ba-doped VPS catalysts, there was no V^{5+} phase detected which could be rationalized that the amount of this particular phase was below the detectable limit of XRD. This is in agreement with the result from redox titration whish showed that the amount of V^{5+} increased as the activation duration increased.

The specific surface area for bulk and Ba-doped VPS catalysts decreased as the activation duration increased. SEM morphologies showed that the longer activated VPS catalysts had more bulky structure, which may cause the decrease in specific surface area. The P/V ratio was higher for bulk and Ba-

doped VPS catalysts with shorter activation duration. Thus, VPS catalysts with shorter activation duration have enhanced phosphorus enriched surface. TPDRO analyses revealed that the increased activation duration could favour higher reactivity and mobility of lattice oxygen.

The optimum activation duration for VPS catalysts activated in 1% O_2/N_2 is 6 hours and further studied on the effect of Mg, Ca and Sr doped VPS catalysts.

Catalytic analysis showed that VPS-Sr achieved optimum *n*-butane conversion and maleic anhydride selectivity as compared to VPS-Mg and VPS-Ca. The catalytic analysis is in agreement with physical, chemical and reactivity analyses. XRD analysis showed that the addition of alkaline-earth metals from Mg to Sr in VPS catalysts could enhance the formation of V^{4+} phases. VPS-Sr has highest specific surface area. This is in agreement with redox titration result which revealed that VPS-Sr has highest amount of V^{4+}. SEM morphologies showed that the plate-like crystals obtained for VPS-Sr have more splits as compared to VPS-Mg and VPS-Ca. TPDRO analyses revealed that the addition of alkaline-earth metal from Mg to Sr induce greater amount of oxygen species removed from the VPS catalysts, which had shown an increased reactivity and mobility of lattice oxygen.

References

Abon, M. et al., 1995. Evolution of a VPO catalyst in *n*-butane oxidation reaction during the activation time. *Journal of Catalysis,* 156, pp. 28 - 36.

Abon, M. and Volta, J.C., 1997. Vanadium phosphorus oxides for *n*-butane oxidation to maleic anhydride. *Applied Catalysis A: General,* 157, pp 173 -193.

Abon, M. and Herrmann, J.M., 2001. Correlation with the redox V^{5+}/V^{4+} ratio in vanadium phosphorus oxide catalysts for mild oxidation of for *n*-butane oxidation to maleic anhydride. *Catalysis Today,* 71, pp. 121 - 128.

Albonetti, S. et al., 1996. A comparison of the reactivity of " nonequilibrated" and "equilibrated" V-P-O catalysts: structural evolution, surface characterization, and reactivity in the selective oxidation of *n*-butane and *n*-pentane. *Journal of Catalysis*, 160, pp. 52 - 64.

Ballarini, N. et al., 2005. The contribution of homogeneous and non-oxidative side reactions in the performance of vanadyl pyrophosphate, catalyst for the oxidation of *n*-butane to maleic anhydride, under hydrocarbon-rich conditions. *Catalysis Today*, 99, pp. 115 – 122.

Bej, S.K. and Rao, M.S., 1992. Selective oxidation of *n*-butane to maleic anhydride. A comparative study between promoted and unpromoted VPO catalysts. *Applied Catalysis A: General,* 83, pp. 149 - 163.

Border, E., 1987. Crystallochemistry of VPO phases and application. *Catalysis Today*, 1, pp. 499 - 526.

Brutovský, M. et al., 1996. Vanadium-Phosphorus Catalysts Modified With Magnesium, Calcium and Barium. *Collection of Czechoslovak Chemical Comminucations*, 62, pp. 1623-1630.

Busca, G. et al., 1986. Nature and mechanism of formation of vanadyl pyrophosphate: active phase in *n*-butane selective oxidation. *Journal of Catalysis*, 99, pp. 400 - 414.

Cavani, F. and Trifirò, F., 1994. Catalyzing butane oxidation to make maleic anhydride. *Chemtech*, 25, pp. 18 - 25.

Cavani, F. and Trifirò, F., 1997. The characterization of the surface properties of V-P-O-based catalysts by probe molecules. *Applied Catalysis A: General*, 157, pp. 195 - 221.

Cavani, F. et al., 2000. Relationship between structural/surface characteristics and reactivity in *n*-butane oxidation to maleic anhydride: The role of V^{3+} species. *Catalysis Today*, 61, pp. 203-210.

Centi, G. et al., 1990. On the polyfunctional nature of $(VO)_2P_2O_7$. *Catalysis Letters*, 4, pp. 309 - 318.

Chauvel, A. et al., 1995. Redox Intercalation of Alkali Metals into Vanadyl Phosphate Dihydrare. *Materials Chemistry and Physics*, 40, pp. 207 - 211.

Cheng, W.H., Wang, W., 1997. Effect of calcination environment on the selective oxidation of n-butane to maleic anhydride over promoted and unpromoted VPO catalysts. *Applied Catalysis A: General*, 156, pp. 57 - 69.

Chilukuri, S., Nimje, R., Pai, S. and Rao, B.S., 2005. Importance of Selectivity in Petrochemical Process. In: Bhattacharyya, K.G. and Talukdar, A.K. (eds.). Catalysis in petroleum and petrochemical industries. New Delhi: Narosa Publishing House., pp 61-72.

Chorkendorff, I. and Niemantsverdriet, J.W., 2003. *Concepts of modern catalysis and kinetics.* 1st ed. Weinheim: Wiley-VCH.

Corma, A. and Garcia, H., 2002. Lewis Acids as Catalysts in Oxidation Reactions: From Homogeneous to Heterogeneous Systems. *Chemical Reviews*, 102 (10), pp. 3837-3892.

Cornaglia, L.M. et al., 2000. Characterisation of cobalt-impregnated VPO Catalysts. *Catalysis Today*, 57, pp. 313 - 322.

Coulston, G.W. et al., 1996. The Kinetic Significance of V^{5+} in *n*-Butane Oxidation Catalysed by Vanadium Phosphates. *Science*, 275, pp. 191 - 193.

Cruz-López, A. et al., 2005. Selective oxidation of butane to maleic anhydride in a catalytic membrane reactor adapted to rich butane feed. *Catalysis Today*, 107-108, pp. 949 - 956.

Datta, A., Agarwal, M. and Dasgupta, S., 2002. Novel vanadium phosphate phases as catalysts for selective oxidation. *Chemical Sciences*. 114 (4), pp. 379 – 390.

Dutta, A., 2005. Selective oxidation of hydrocarbons using vanadium phosphates. In: Bhattacharyya, K.G. and Talukdar, A.K. (eds.). Catalysis in petroleum and petrochemical industries. New Delhi: Narosa Publishing House., pp 53-60.

Duvauchelle, N. and Bordes, E., 1999. Influence of the nanostructure and morphology of $(VO)_2P_2O_7$ on its catalytic reactivity. *Catalysis Letters*, 57, pp. 81 - 88.

Esteman, E., Merzouk, M., Taouk, B., Borders, E., Contractor, R., 1995. Systematic control of crystal morphology during preparation of selective vanadyl pyrophosphate. In: Poncelet G., Martens J., Delman B., Jacobs P.A., Grange P. (1st Ed.) Preparation of Catalysts VI (pp 707-716). Amterdam: Elsevier.

Gascón, J. et al., 2006. A generalized kinetic model for the partial oxidation of *n*-butane to maleic anhydride under aerobic and anaerobic conditions. *Chemical Engineering Sceince*, 61, pp. 6385 - 6394.

Goh, C.K. et al., 2008. Influence of Bi-Fe additive on properties of vanadium phosphate catalysts for n-butane oxidation to maleic anhydride. *Catalysis Today*, 131, pp. 408 - 412.

Govender, N., Friedrich, H.B. and Van Vuuren, M.J., 2004. Controlling factors in the selective conversion of *n*-butane over promoted VPO catalysts at low temperature. *Catalysis Today*, 97, pp. 315-324.

Guan, J. et al., 2008. Selective oxidation of isobutene and isobutene over vanadium phosphorus oxides. *Catalysis Communication*, 10, pp. 276 - 280.

Guliants, V.V. et al., 1995. Evolution of the active surface of the vanadyl pyrophosphate catalysts. *Catalysis Letter*, 32, pp. 379 - 386.

Guliants, V. V. and Carreon, M. A., 2005. Vanadium-Phosphorus-Oxides: from fundamentals of *n*-butane oxidation to synthesis of new phases. *Catalysis*, 18, pp. 1 - 45.

Hagen, J., 2006. *Industrial catalysis*, 2nd ed. Weinheim: Wiley-VCH

Haber, J. et al., 1997. Mechanochemistry: The activation method of VPO catalysts for *n*-butane partial oxidation. *Catalysis Today*, 33 (1-3), pp. 39-47.

Hodnett, B.K. and Delmon, B., 1984. Influence of reductive pretreatments on the activity and selectivity of vanadium-phosphorus oxide catalysts for *n*-butane partial oxidation. *Industrial and Engineering Chemistry Fundamentals*, 23, pp. 465-470.

Hutchings, G.J. and Higgins, R., 1996. Effect of promoters on the selective oxidation of n-butane with vanadium phosphorus oxide catalysts. *Journal of Catalysis*, 162, pp. 153 - 168.

Hutchings, G.J. et al., 1997 Improved method of preparation of vanadium phosphate catalyst. *Catalysis Today*, 33, pp. 161 - 171.

Hutchings, G.J., 2001. Promotion in heterogeneous catalysis: a topic requiring a new approach? *Catalysis Letters*, 75, pp. 1 - 12.

Irmawati, R. et al., 2004. Effect of calcination temperatures on physicochemical properties of vanadium-antimony mixed oxide catalysts. *Catalysis Today*, 93-95, pp. 631 - 637.

Ishimura, T., Sugiyama, S., Hayashi, H., 2000. Vanadyl hydrogenphosphate sesquihydrate as a precursor for preparation of $(VO)_2P_2O_7$ and cobalt-incorporated catalysts. *Journal of Molecular Catalysis. A: Chemical*, 158, pp. 559 - 565.

Kalevaru, V.N., Madaan, N., Martin, A., 2011. Synthesis, characterization and catalytic performance of titania supported VPO catalysts for the ammoxidation of 3-picoline. *Applied Catalysis*, 391, pp. 52 - 62.

Kiely, C.J. et al., 1996. Characterisation of variations in vanadium phosphate catalyst microstructure with preparation route. *Journal of Catal*ysis, 162, pp. 31 - 47.

Klug, P.H. and Alexander, E., 1974. *X-ray diffraction procedures for polycrystalline and amorphous materials*, 2nd ed. New York: John Wiley & Sons.

Lee, Amanda., 2000, *Manufacturing Maleic Anhydride* [Online]. Available at: http://www.che.lsu.edu/COURSES/4205/2000/Lee/paper.htm
[Accessed: 13 May 2010].

Mallada, R. et al., 2000. Influence of the reaction atmosphere on the characteristics and performance of VPO catalysts. *Journal of Catalysis*, 196, pp. 1 - 7.

Matsuura, I., 1992. Vanadyl Pyrophosphate as A Selective Oxidation Catalyst. *Studies in Surface Science and Catalysis*, 72, pp. 247 - 254.

Niwa, M. and Murakami, Y., 1982. Reaction mechanism of Ammoxidation of Toluene: IV oxidation state of vanadium oxide and its reactivity for toluene oxidation. *Journal of Catalysis*, 76, pp. 9 - 16.

Patience, G.S. and Bockrath, R.E., 2010. Butane oxidation process development in a circulating fluidized bed. *Applied Catalysis A: General*, 376, pp. 4 - 12.

Pierini, B., Lombardo, E.A., 2005. Cr, Mo and W used as promoters in the partial oxidation of n-butane to maleic anhydride. *Catalysis Today*, 107-108, pp. 323 - 329.

Poli, G. et al., 1981. The chemistry of catalysts based on vanadium-phosphorus oxides: Note II: The role of the method of preparation. *Applied Catalysis*, 1, pp. 395 - 404.

Pries de Oliveira, P.G. et al., 2000. Modification of vanadium phosphorus oxide used for *n*-butane oxidation to maleic anhydride by interaction with niobium phosphate. *Catalysis Today*, 57, pp. 177 - 186.

Redhead P. A., 1962. Thermal desorption of gases. *Vacuum* 12, pp. 203 - 211.

Rownaghi, A.A. and Taufiq-Yap, Y.H., 2009. Influence of rare-earth and bimetallic promoters on various VPO catalysts for partial oxidation of *n*-butane. *Catalysis Letter*, 130, pp. 504 - 516.

Sakakini, B.H., Taufiq-Yap, Y.H. and Waugh, K.C., 2000. A study of the kinetics and mechanism of the adsorption and anaerobic oxidation of *n*-butane over a vanadyl pyrophosphate catalyst. *Journal of Catalysis*, 189, pp. 253 - 262.

Sartoni, L. et al., 2004. Promotion of vanadium phosphate catalysts using gallium compounds: effect of low Ga/V molar ratios. *Journal of Molecular Catalysis A: Chemical*, 220, pp. 85 - 92.

Schiøtt, B. and Jørgensen, K.A., 1993. The Oxidative Species on a Vanadyl Pyrophosphate Surface. A Model for Some Steps in the Maleic Anhydride Synthesis. *Catalysis Today*, 16, pp. 79 - 90.

Shima, K. and Hatano, M., 1997. Maleic anhydride by heterogeneous oxidation of *n*-butane. *App. Surf. Sci*, 121/122, pp. 452 - 460.

Sivasanker, S., 2002. Recent development in catalysis. In: Catalysis principles and applications. 1st Edition. (pp 271-288). New Delhi: Narosa Publishing House.

Sri Consulting., 2011, *World Petrochemical Report: Maleic Anhydride* [Online]. Available at: http://www.sriconsulting.com/WP/Public/Reports/ma/ [Accessed: 30 July 2011].

Taufiq-Yap, Y.H. et al., 2001. The effect of the duration of *n*-butane/air pretreatment on the morphology and reactivity of $(VO)_2P_2O_7$ catalysts. *Catalysis Letters*, 74, pp. 99 - 104.

Taufiq-Yap, Y.H. et al., 2003. Bismuth-modified vanadyl pyrophosphate catalysts. *Catalysis Letter*, 89, pp. 87 - 93.

Taufiq-Yap, Y.H. et al., 2004. Synthesis and characterization of vanadyl pyrophosphate catalysts via vanadyl hydrogen phosphate sesquihydrate precursor. *Catalysis Today*, 93-95, pp. 715 - 722.

Taufiq-Yap, Y.H., 2006. Effect of Cr and Co promoters addition on vanadium phosphate catalysts for mild oxidation of n-butane. *Journal of Natural Gas Chemistry*, 15, pp. 144 - 148.

Taufiq-Yap, Y.H., Kamiya, Y. and Tan, K.P., 2006. Promotional Effect of Bismuth as Dopant in Bi-Doped Vanadyl Pyrophosphate Catalysts for Selective Oxidation of *n*-Butane to Maleic Anhydride. *Journal of Natural Gas Chemistry*, 15, pp. 297 - 302.

Taufiq-Yap, Y.H. and Saw, C.S., 2008. Effect of calcinations environments on the vanadium phosphate catalysts for selective oxidation of propane and *n*-butane. *Catalysis Today*, 131, pp. 285 - 291.

Trivedi, B.C. and Culbertson, B.M., 1982. *Maleic anhydride*, 1st ed. New York: Plenum Press.

Volta, J.C., 2000. Vanadium phosphorus oxides, a reference catalyst for mild oxidation of light alkanes: a review. *C. R. Acad. Sci. Series IIC-Chemistry*, 3, pp. 717 - 723.

Zazhigalov, V.A. et al., 1996. *n*-Butane oxidation on V-P-O catalysts. Influence of alkali and alkali-earth metal ions as additions. *Applied Catalysis*, 134, pp. 225 - 237.

APPENDIX A

Preparation for Alkaline Earth Metal-doped Vanadyl Pyrophosphosphate Catalyst

A total of 10.00g of $VOPO_4 \cdot 2H_2O$ was used in the synthesis of magnesium-doped vanadyl pyrophosphosphate catalyst.

Given the molecular weight of the starting materials as below:
$VOPO_4 \cdot 2H_2O$ = 197.94 g mol-1
$Mg(NO_3)_2 \cdot 6H_2O$= 256.41 g mol^{-1}
Number of moles of $VOPO_4 \cdot 2H_2O$ used = 10g/ 197.9426 g mol^{-1}
= 0.05052 mol

For 3 % Magnesium-doped VPS catalysts (VPS-Mg)

$$\frac{Mg}{V} = \frac{3}{100} = 0.03$$

Molecular weight of $Mg(NO_3)_2 \cdot 6H_2O$ = 256.41 g mol^{-1}
Number of moles of Mg needed = 0.03 X 0.05052 mol
= 1.5156×10^{-3} mol

Mass of $Mg(NO_3)_2 \cdot 6H_2O$ = 1.5156×10^{-3} mol × 256.41 g mol^{-1}
= 0.3886 g

For 3 % Calcium-doped VPS catalysts (VPS-Ca)

$$\frac{Ca}{V} = \frac{3}{100} = 0.03$$

Molecular weight of $Ca(NO_3)_2 \cdot 4H_2O$ = 236.15 g mol^{-1}
Number of moles of Ca needed = 0.03 X 0.05052 mol
= 1.5156×10^{-3} mol

Mass of $Ca(NO_3)_2 \cdot 4H_2O$ = 1.5156×10^{-3} mol × 236.15 g mol^{-1}
= 0.3579 g

For 3 % Strontium-doped VPS catalysts (VPS-Sr)

$$\frac{Sr}{V} = \frac{3}{100} = 0.03$$

Molecular weight of anhydrous $Sr(NO_3)_2$ = 211.63 g mol^{-1}

Number of moles of Sr needed = 0.03 X 0.05052 mol

= 1.5156×10^{-3} mol

Mass of anhydrous $Sr(NO_3)_2$ = 1.5156×10^{-3} mol × 211.63 g mol^{-1}

= 0.3207 g

For 1 % Barium-doped VPS catalysts (VPS-Ba)

$$\frac{Ba}{V} = \frac{1}{100} = 0.01$$

Molecular weight of $Ba(NO_3)_2$ = 261.36 g mol^{-1}

Number of moles of Ba needed = 0.01 X 0.05052 mol

= 5.0520×10^{-4} mol

Mass of anhydrous $Sr(NO_3)_2$ = 5.0520×10^{-4} mol × 261.36 g mol^{-1}

= 0.132 g

APPENDIX B

Preparation of Solution Used in Redox Titration

(i) Preparation of 2M sulphuric acid, H_2SO_4 solution

The stock solution used in preparation is concentrated H_2SO_4 (95-98%).

Given the density and molecular weight of 95-98% H_2SO_4 as below:
ρ of 95-98% H_2SO_4 = 1.84 g cm^{-3}
M_r of 95-98% H_2SO_4 = 98.07 g mol^{-1}

$$\frac{1.84 \text{ g cm}^{-3}}{98.07 \text{ g mol}^{-1}} \text{ X } \frac{95}{100} \text{ X } 1000$$

Molarity of 95-98% H_2SO_4= 98.07 g mol^{-1}

To prepare 2M H_2SO_4, the following formula is applied.

$$M_1V_1 = M_2V_2$$

Where M_1 = molarity of 95-98% H_2SO_4 (17.82 M)
M_2 = molarity of diluted H_2SO_4 (2 M)
V_1 = volume of 95-98% H_2SO_4
V_2 = volume of diluted H_2SO_4 (1000 cm^3)

(17.82 M) (V_1) = (2 M) (1000 cm^3)
V_1 = 112.23 cm^3

(ii) Preparation of 0.1 M sulphuric acid, H_2SO_4 solution

To prepare 0.1 M H_2SO_4, the following formula is applied.

$$M_1V_1 = M_2V_2$$

Where M_1 = molarity of 95-98% H_2SO_4 (17.82 M)
M_2 = molarity of diluted H_2SO_4 (2 M)
V_1 = volume of 95-98% H_2SO_4
V_2 = volume of diluted H_2SO_4 (1000 cm^3)

(17.82 M) (V_1) = (0.1 M) (1000 cm^3)
V_1 = 5.61 cm^3

(iii) Preparation of 0.01 N of potassium permanganate, $KMnO_4$

$$MnO_4^- + 8\ H^+ + 5\ e^- \leftrightarrow Mn^{2+} + 4\ H_2O$$

To convert normality to molarity, the following formula is applied.

$$\text{Molarity of } KMnO_4,\ M\ (\text{mol } L^{-1}) = \frac{N\ (\text{eq } L^{-1})}{n\ (\text{eq mol}^{-1})}$$

$$= \frac{0.01}{5}$$

$$= 0.002\ M$$

Given the molecular weight of $KMnO_4$ is 158.04 g mol^{-1},

Weight of KMnO4 needed = 0.002 M × 158.04 g mol^{-1}
= 0.3161 g

(iv) Preparation of 0.01 N of ammonium iron(II) sulphate, $(NH_4)_2Fe(SO_4)_2{\cdot}6H_2O$

$$Fe^{2+} + e^- \leftrightarrow Fe^{3+}$$

To convert normality to molarity, the following formula is applied.

$$\text{Molarity of } (NH_4)_2Fe(SO_4)_2{\cdot}6H_2O,\ M\ (\text{mol } L^{-1}) = \frac{0.01}{1}$$

$$= \frac{N\ (\text{eq } L^{-1})}{n\ (\text{eq mol}^{-1})} \frac{0.01}{1}$$

$$= 0.01\ M$$

Given the molecular weight of $KMnO_4$ is 391.99 g mol^{-1},

Weight of $KMnO_4$ needed = 0.01 M × 391.99 g mol^{-1}
= 3.9199 g

(v) Preparation of Diphenylamine, Ph2NH indicator

1 g of diphenylamine was weighed and dissolved in a few mL of concentrated sulphuric acid, H_2SO_4. Then, the solution was transferred to a 100 mL volumetric flask and was topped up to 100 mL using concentrated H_2SO_4.

APPENDIX C

Crystallite Size Measurements by Using Powder XRD Technique

Crystallite size, T is given by Debye-Scherrer equation,

$$T(A) = \frac{0.89\,\lambda}{FWHM\,(rad) \times \cos\theta}$$

Given $\lambda_{Cu\,K\alpha} = 1.54$ A,

$$FWHM\,(rad) = FWHM\,(^\circ) \times \frac{\pi}{180^\circ}$$

For VPS-6

2θ (°)	θ (°)	FWHM (°)	FWHM (rad)	T (Å)
22.5600	11.2800	2.1000	0.03666	38.1232
28.5311	14.2656	0.6889	0.01203	117.5568
29.9000	14.9500	0.6400	0.01117	127.0025

For VPS-18

2θ (°)	θ (°)	FWHM (°)	FWHM (rad)	T (Å)
22.6400	11.3200	1.7710	0.03091	45.2214
28.3719	14.1860	0.6508	0.01136	124.4464
29.7572	14.8786	0.6104	0.01065	133.1594

For VPS-30

2θ (°)	θ (°)	FWHM (°)	FWHM (rad)	T (Å)
22.8741	11.4371	1.5282	0.02668	52.4126
28.6909	14.3455	0.5868	0.01024	138.1554
30.1126	15.0563	0.5803	0.01013	140.1109

For VPS-75

2θ (°)	θ (°)	FWHM (°)	FWHM (rad)	T (Å)
22.9600	11.4800	1.4088	0.02459	56.8760
28.6782	14.3391	0.7603	0.01327	106.6067
30.1266	15.0633	0.5867	0.01024	138.6104

For VPS-Ba 6

2θ (°)	θ (°)	FWHM (°)	FWHM (rad)	T (Å)
22.6690	11.3345	1.7477	0.03051	45.8166
28.4438	14.2219	0.7080	0.01236	114.3960
29.8800	14.9400	0.6564	0.01146	123.7829

For VPS-Ba 18

2θ (°)	θ (°)	FWHM (°)	FWHM (rad)	T (Å)
22.7180	11.3590	1.4230	0.02484	56.2795
28.4406	14.2203	0.6638	0.01159	121.9952
29.8984	14.9492	0.6353	0.01109	127.9182

For VPS-Ba 30

2θ (°)	θ (°)	FWHM (°)	FWHM (rad)	T (Å)
22.6713	11.3357	1.4139	0.02468	56.6397
28.4080	14.2040	0.6736	0.01176	120.2230
29.8479	14.9240	0.6558	0.01145	123.8818

For VPS-Ba 75

2θ (°)	θ (°)	FWHM (°)	FWHM (rad)	T (Å)
22.7417	11.3709	1.2586	0.02197	63.6341
28.4335	14.2168	0.6870	0.01199	117.9252
29.8912	14.9456	0.6518	0.01138	124.6589

For VPS-Mg

2θ (°)	θ (°)	FWHM (°)	FWHM (rad)	T (Å)
22.6416	11.3208	1.6805	0.02933	47.6576
28.4482	14.2241	0.6769	0.01182	119.6234
29.8974	14.9487	0.6927	0.01209	117.3374

For VPS-Ca

2θ (°)	θ (°)	FWHM (°)	FWHM (rad)	T (Å)
22.6572	11.3286	1.7656	0.03082	45.3548
28.4458	14.2229	0.7108	0.01241	113.9356
29.8202	14.9101	0.8004	0.01397	101.5286

For VPS-Sr

2θ (°)	θ (°)	FWHM (°)	FWHM (rad)	T (Å)
22.6235	11.3118	1.9449	0.03395	41.1709
28.4469	14.2235	0.7657	0.01337	105.7550
29.8494	14.9247	0.7949	0.01388	102.1939

APPENDIX D

Redox Titration

According to Niwa and Murakami (1982),

$T_1 = V^{4+} + 2V^{3+} = 20 [MnO_4^-] V_1$ (1)
$T_2 = V^{5+} + V^{4+} + V^{3+} = 20 [Fe^{2+}] V_2$ (2)
$T_3 = V^{5+} = 20 [Fe^{2+}] V_3$ (3)

Subtract (2) with (3),
$V^{4+} + V^{3+} = 20 [Fe^{2+}] V_2 - 20 [Fe^{2+}] V_3$ (4)

Subtract (1) with (4),
$V^{3+} = 20 [MnO4-] V1 - 20 [Fe2+] V2 + 20 [Fe2+] V3$ (5)

Substitute (5) into (1),
V4+ + 2(20 [MnO4-] V1 - 20 [Fe2+] V2 + 20 [Fe2+] V3) = 20 [MnO4-] V1
V4+ = 20 [MnO4-] V1 - 40 [MnO4-] V1 + 40 [Fe2+] V2 - 40 [Fe2+] V3
= 40 [Fe2+] V2 - 40 [Fe2+] V3 - 20 [MnO4-] V1 (6)

Substitute (5) and (6) into (2),
$20 [Fe^{2+}] V_2 = V^{5+} + (40 [Fe^{2+}] V_2 - 40 [Fe^{2+}] V_3 - 20 [MnO_4^-] V_1) + (20 [MnO_4^-] V_1 - 20 [Fe^{2+}] V_2 + 20 [Fe^{2+}] V_3)$

$V^{5+} = 20 [Fe^{2+}] V_3$ (7)

From (5),
$V^{3+} = 20 (0.01) V_1 – 20 (0.01) V_2 + 20 (0.01) V_3$
$= 0.2 V_1 – 0.2 V_2 + 0.2 V_3$ (8)

From (6),
$V^{4+} = 40 (0.01) V_1 – 40 (0.01) V_2 - 20 (0.01) V_3$
$= 0.4 V_2 – 0.4 V_3 - 0.2 V_1$ (9)

From (7),
$V^{5+} = 20 (0.01) V_3$
$= 0.2 V_3$ (10)

Therefore, the average vanadium valence is calculated as,

$$V_{AV} = \frac{3V^{3+} + 4V^{4+} + 5V^{5+}}{V^{3+} + V^{4+} + V^{5+}} \quad (11)$$

For VPS Bulk-6

Given $V_1 = 7.90$, $V_2 = 10.20$, $V_3 = 2.20$,

From (9),
$V^{4+} = 0.4\ V_2 – 0.4\ V_3 - 0.2\ V_1$
$= 0.4\ (10.20) – 0.4\ (2.20) - 0.2\ (7.90)$
$= 1.620$

From (10),
$V^{5+} = 0.2\ V_3$
$= 0.2\ (2.20)$
$= 0.440$

Substitute the values of V^{4+} and V^{5+} into (11),

$$V_{AV} = \frac{4V^{4+} + 5V^{5+}}{V^{4+} + V^{5+}}$$

$$= \frac{4(1.620) + 5(0.440)}{1.620 + 0.440}$$

$= 4.2136$

Table: Average oxidation numbers of vanadium for bulk VPS catalysts obtained via redox titration.

	Volume, V/ cm^3	Volume of $KMnO_4$, (V_1)/ cm^3			Volume of $(NH_4)_2Fe(SO_4)_2$, (V_2)/ cm^3			Volume of $(NH_4)_2Fe(SO_4)_2$, (V_3)/ cm^3		
		1	2	3	1	2	3	1	2	3
VPS Bulk-6	Initial, V_i	9.90	20.20	27.20	23.80	10.10	22.90	32.80	23.10	22.50
	Final, V_f	17.70	27.20	35.10	33.40	20.30	33.10	35.00	25.30	24.70
	Volume Used	7.80	8.00	7.90	10.20	10.20	10.20	2.20	2.20	2.20
	Average		7.90			10.20			2.20	
VPS Bulk-18	Initial, V_i	8.70	18.50	30.00	2.00	13.80	12.00	25.70	28.20	28.00
	Final, V_f	17.70	27.50	39.00	13.80	25.70	13.80	28.50	31.10	30.70
	Volume Used	9.00	9.00	9.00	11.80	11.90	11.80	2.80	2.90	2.70
	Average		9.00			11.83			2.80	
VPS Bulk-30	Initial, V_i	27.50	30.00	6.00	34.70	10.00	25.00	11.00	16.00	20.00
	Final, V_f	35.20	37.70	13.70	45.80	21.00	36.10	14.40	19.30	23.30
	Volume Used	7.70	7.70	7.70	11.10	11.00	11.10	3.40	3.30	3.30
	Average		7.70			11.07			3.33	
VPS Bulk-75	Initial, V_i	2.20	9.00	17.00	8.00	15.00	10.00	27.40	10.00	20.00
	Final, V_f	8.50	15.20	23.20	20.40	27.60	22,50	33.80	16.30	26.40
	Volume Used	6.30	6.20	6.20	12.40	12.60	12.50	6.40	6.30	6.40
	Average		6.23			12.50			6.27	

Sample	V_1	V_2	V_3	V^{3+}	V^{4+}	V^{5+}	V_{av}
VPS Bulk-6	7.90	10.20	2.20	-0.020	1.620	0.440	4.21
VPS Bulk-18	9.00	11.83	2.80	-0.006	1.812	0.560	4.24
VPS Bulk-30	7.70	11.07	3.33	-0.008	1.556	0.666	4.30
VPS Bulk-75	6.23	12.50	6.27	0.000	1.246	1.254	4.50

Table: Average oxidation numbers of vanadium for 1% Ba-doped VPS catalysts obtained via redox titration

	Volume, V/ cm^3	Volume of $KMnO_4$, (V_1)/ cm^3			Volume of $(NH_4)_2Fe(SO_4)_2$, (V_2)/ cm^3			Volume of $(NH_4)_2Fe(SO_4)_2$, (V_3)/ cm^3		
		1	2	3	1	2	3	1	2	3
VPS Ba-6	Initial, V_i	3.00	10.00	20.00	5.00	15.00	26.20	3.40	8.20	15.00
	Final, V_f	8.70	15.90	25.80	14.00	24.10	35.20	6.40	11.10	17.90
	Volume Used	5.70	5.90	5.80	9.00	9.10	9.00	3.00	2.90	2.90
	Average		5.80			9.03			2.93	
VPS Ba-18	Initial, V_i	3.50	15.30	27.00	2.00	16.00	5.60	2.00	10.00	16.00
	Final, V_f	12.70	24.50	36.20	15.70	29.60	19.20	6.60	14.50	20.40
	Volume Used	9.20	9.20	9.20	13.70	13.60	13.60	4.60	4.50	4.40
	Average		9.20			13.63			4.40	
VPS Ba-30	Initial, V_i	2.00	10.00	20.00	4.30	18.00	32.00	2.00	10.40	16.00
	Final, V_f	9.80	17.90	27.70	16.80	30.40	44.40	6.60	15.00	20.60
	Volume Used	7.80	7.90	7.70	12.50	12.40	12.40	4.60	4.60	4.60
	Average		7.80			12.43			4.60	
VPS Ba-75	Initial, V_i	3.00	12.00	20.00	3.00	20.00	5.20	6.00	15.00	25.00
	Final, V_f	10.30	19.30	27.20	17.50	34.40	19.60	13.00	22.00	31.90
	Volume Used	7.30	7.30	7.20	14.50	14.40	14.40	7.00	7.00	6.90
	Average		7.27			14.43			6.97	

Sample	V_1	V_2	V_3	V^{3+}	V^{4+}	V^{5+}	V_{av}
VPS Ba-6	5.80	9.03	2.93	-0.06	1.28	0.586	4.31
VPS Ba-18	9.20	13.63	4.40	-0.006	1.852	0.88	4.32
VPS Ba-30	7.80	12.43	4.60	-0.006	1.572	0.92	4.37
VPS Ba-75	7.27	14.43	6.97	-0.038	1.53	1.394	4.48

Table: Average oxidation numbers of vanadium for alkaline earth metals-doped VPS catalysts obtained via redox titration

	Volume, V/ cm^3	Volume of $KMnO_4$, (V_1)/ cm^3			Volume of $(NH_4)_2Fe(SO_4)_2$, (V_2)/ cm^3			Volume of $(NH_4)_2Fe(SO_4)_2$, (V_3)/ cm^3		
		1	2	3	1	2	3	1	2	3
VPS-Mg	Initial, V_i	5.00	14.20	23.00	3.00	15.00	7.40	4.00	10.10	15.00
	Final, V_f	12.20	21.20	30.10	13.60	25.50	17.90	7.30	13.40	18.40
	Volume Used	7.20	7.00	7.10	10.60	10.50	10.50	3.30	3.30	3.40
	Average		7.10			10.53			3.30	
VPS-Ca	Initial, V_i	7.50	18.00	25.50	6.40	3.00	10.30	1.00	10.40	21.00
	Final, V_f	15.70	26.30	33.80	17.70	14.30	21.60	3.90	13.20	23.70
	Volume Used	8.20	8.30	8.30	11.30	11.30	11.30	2.90	2.80	2.70
	Average		8.27			11.30			2.80	
VPS-Sr	Initial, V_i	11.00	19.30	27.60	9.20	21.00	5.30	6.00	8.40	11.20
	Final, V_f	17.30	25.70	34.00	18.20	29.90	14.30	8.20	10.60	13.40
	Volume Used	6.30	6.40	6.40	9.00	8.90	9.00	2.20	2.20	2.20
	Average		6.37			8.97			2.20	

Sample	V_1	V_2	V_3	V^{3+}	V^{4+}	V^{5+}	V_{av}
VP-Mg	7.10	10.53	3.30	-0.026	1.472	0.66	4.31
VPS-Ca	8.27	11.30	2.80	-0.046	1.746	0.56	4.24
VPS-Sr	6.37	8.97	2.20	-0.080	1.434	0.44	4.23

APPENDIX E

Inductive-Coupled Plasma-Optical Emission Spectroscopy (ICP-OES)

Stock Solution for Phosphorus (Ammonium Dihydrogen *Ortho*phosphate, $NH_4H_2PO_4$)

Relative Molecular Mass of $NH_4H_2PO_4$ = 115.03 g/mol
Relative Atomic Mass of P =30.97 g/mol
50 ppm of P= 50 mg/L= 0.05g/L

$$\text{Mole of P} = \frac{0.05 \text{ g L}^{-1}}{30.97 \text{ g mol}^{-1}}$$

$$= 1.6145 \text{ X } 10^{-3} \text{ mol}$$

Mass of $NH_4H_2PO_4$= $1.6145 \text{ X } 10^{-3}$ mol X 115.03 g/mol
= 0.1857g
The stock solution was prepared by dissolving 0.1857g of $NH_4H_2PO_4$ in H_2O and top up to 1L.

Standard Solution for Phosphorus

Standard Solution	Volume of Stock Solution Needed (mL)
10 ppm	50
20 ppm	100
30 ppm	150

Volume of Stock Solution + 10mL 8M HNO_3, top up to 250mL.

$M_1V_1 = M_2V_2$
50 ppm (V_1) = (10 ppm) (250mL)
V_1 = 50 mL

Stock Solution for Phosphorus (Ammonium Metavanadate, NH_4VO_3)

Relative Molecular Mass of NH_4VO_3= 116.98 g/mol
Relative Atomic Mass of V=50.94 g/mol
50 ppm of V= 50 mg/L= 0.05g/L

$$\text{Mole of V} = \frac{0.05 \text{ g L}^{-1}}{50.94 \text{ g mol}^{-1}}$$

$$= 9.8155 \text{ X } 10^{-4} \text{ mol}$$

Mass of NH_4VO_3 = 9.8155 X 10^{-4} mol X 116.98 g/mol
= 0.1148g

The stock solution was prepared by dissolving 0.1148g of NH_4VO_3 in H_2O and top up to 1L.

Standard Solution for Vanadium

Standard Solution	Volume of Stock Solution Needed (mL)
10 ppm	50
20 ppm	100
30 ppm	150
40 ppm	200

Volume of Stock Solution + 10mL 8M HNO_3, top up to 250mL.

$M_1V_1 = M_2V_2$
50 ppm (V_1) = (10 ppm) (250mL)
V_1 = 50 mL

Preparation of 8M Nitric Acid, HNO_3

$$\text{Molarity of } HNO_3 = \frac{\text{Density of } HNO_3}{\text{RMM of } HNO_3} \times \frac{65}{100} \times 1000$$

$$= \frac{1.39 \text{gcm}^{-3}}{63.01 \text{gmol}^{-1}} \times \frac{65}{100} \times 1000$$

= 14.339M

$M_1V_1 = M_2V_2$
14.339M (V_1) = 8M (250mL)
V_1= 139.48mL

Sample Preparation
To prepare 100 ppm of sample,
10mL of 8M HNO_3 was added to 0.025 g of sample and heated for about 2 minutes. The mixture was then top up to 250mL in volumetric flask.

Blank Solution
10mL of 8M HNO_3 was top up to 250mLof deionised water in volumetric flask.

Stock Solution for Magnesium ($Mg(NO_3)_2.6H_2O$)
Relative Molecular Mass of $Mg(NO_3)_2.6H_2O$ = 256.41 g/mol
Relative Atomic Mass of Mg=24.305 g/mol
50 ppm of V= 50 mg/L= 0.05g/L

$$\text{Mole of Mg} = \frac{0.05\text{g L}^{-1}}{24.305\text{gmol}^{-1}}$$
$$= 2.057 \text{ X } 10^{-3} \text{ mol}$$

Mass of $Mg(NO_3)_2.6H_2O$ =$2.057 \text{ X } 10^{-3}$ mol X 256.41 g/mol
= 0.5274g

The stock solution was prepared by dissolving 0.5274g of $Mg(NO_3)_2.6H_2O$ in H_2O and top up to 1L.

Standard Solution for Magnesium

Standard Solution	Volume of Stock Solution Needed (mL)
1 ppm	5
2 ppm	10
3 ppm	15
5 ppm	25

Volume of Stock Solution + 10mL 8M HNO_3, top up to 250mL.

$M_1V_1 = M_2V_2$
50 ppm (V_1) = (1 ppm) (250mL)
V_1 = 5 mL

Stock Solution for Calcium ($Ca(NO_3)_2.4H_2O$)
Relative Molecular Mass of $Ca(NO_3)_2.4H_2O$ = 236.15 g/mol
Relative Atomic Mass of Ca = 40.078 g/mol
50 ppm of V= 50 mg/L= 0.05g/L

$$\text{Mole of Ca} = \frac{0.05\text{g L}^{-1}}{40.078\text{gmol}^{-1}}$$
$$= 1.248 \text{ X } 10^{-3} \text{ mol}$$

Mass of $Ca(NO_3)_2.4H_2O$ =$1.248 \text{ X } 10^{-3}$ mol X 236.15 g/mol
= 0.2947g

The stock solution was prepared by dissolving 0.2947g of $Ca(NO_3)_2.4H_2O$ in H_2O and top up to 1L.

Standard Solution for Calcium

Standard Solution	Volume of Stock Solution Needed (mL)
1 ppm	5
2 ppm	10
3 ppm	15
5 ppm	25

Volume of Stock Solution + 10mL 8M HNO_3, top up to 250mL.

$M_1V_1 = M_2V_2$
50 ppm (V_1) = (1 ppm) (250mL)
V_1 = 5 mL

Stock Solution for Strontium ($Sr(NO_3)_2$)
Relative Molecular Mass of $Sr(NO_3)_2$= 211.63 g/mol
Relative Atomic Mass of Sr = 87.62 g/mol
50 ppm of V= 50 mg/L= 0.05g/L

$$\text{Mole of Sr} = \frac{0.05\text{g L}^{-1}}{87.62\text{gmol}^{-1}}$$

$= 5.706 \times 10^{-4}$ mol

Mass of $Sr(NO_3)_2$ $= 5.706 \times 10^{-4}$ mol X 211.63 g/mol
= 0.1208g

The stock solution was prepared by dissolving 0.1208g of $Sr(NO_3)_2$ in H_2O and top up to 1L.

Standard Solution for Strontium

Standard Solution	Volume of Stock Solution Needed (mL)
1 ppm	5
2 ppm	10
3 ppm	15
4 ppm	20
5 ppm	25

Volume of Stock Solution + 10mL 8M HNO_3, top up to 250mL.

$M_1V_1 = M_2V_2$
50 ppm (V_1) = (1 ppm) (250mL)
V_1 = 5 mL

Stock Solution for Barium ($Ba(NO_3)_2$)

Relative Molecular Mass of $Ba(NO_3)_2$= 261.36g/mol

Relative Atomic Mass of Ba = 137.33 g/mol

50 ppm of V= 50 mg/L= 0.05g/L

$$\text{Mole of Ba} = \frac{0.05\text{g L}^{-1}}{137.33\text{gmol}^{-1}}$$

$= 3.641 \text{ X } 10^{-4}$ mol

Mass of $Ba(NO_3)_2$=$3.641 \text{ X } 10^{-4}$ mol X 261.36 g/mol

= 0.0952g

The stock solution was prepared by dissolving 0.0952g of $Ba(NO_3)_2$ in H_2O and top up to 1L.

Standard Solution for Barium

Standard Solution	Volume of Stock Solution Needed (mL)
0.5 ppm	2.5
1.0 ppm	5.0
1.5 ppm	7.5
2.0 ppm	10.0
2.5 ppm	12.5

Volume of Stock Solution + 10mL 8M HNO_3, top up to 250mL.

$M_1V_1 = M_2V_2$

50 ppm (V_1) = (0.5 ppm) (250mL)

V_1 = 2.5 mL

Table: Chemical analyses using ICP-OES

Sample	Vanadium Concentration (mg/L)	Phosphorus Concentration (mg/L)	Vanadium Concentration (g/L)	Phosphorus Concentration (g/L)	Mole of V	Mole of P	P/V
VPS Bulk-6	40.56	30.64	0.04056	0.03064	0.0007962	0.0009892	1.24
VPS Bulk-18	41.35	24.82	0.04135	0.02482	0.0008117	0.0008013	0.99
VPS Bulk-30	42.03	23.69	0.04203	0.02369	0.0008251	0.0007648	0.93
VPS Bulk-75	41.59	21.70	0.04159	0.0217	0.0008164	0.0007006	0.86
VPS Ba-6	40.47	24.96	0.04047	0.02496	0.0007944	0.0008058	1.01
VPS Ba-18	40.99	23.90	0.04099	0.02390	0.0008046	0.0007716	0.96
VPS Ba-30	42.03	25.40	0.04203	0.02540	0.0008251	0.0008200	0.99
VPS Ba-75	41.87	24.78	0.04187	0.02478	0.0008219	0.0008000	0.97
VPS-Mg	40.02	22.96	0.04002	0.02296	0.0007856	0.0007413	0.94
VPS-Ca	41.21	24.34	0.04121	0.02434	0.0008090	0.0007858	0.97
VPS-Sr	40.89	23.06	0.04089	0.02306	0.0008027	0.0007445	0.93

Appendix F

Temperature Programmed Desorption (TPD) Calculation

For VPS 6,

Total oxygen desorbed= 3.465×10^{-4} mol g^{-1}

Total oxygen atom desorbed= 3.465×10^{-4} mol $g^{-1} \times 6.02 \times 10^{23}$ atom mol^{-1}
$= 2.086 \times 10^{20}$ atom g^{-1}

Desorption Activation Energy, $E_d = RT_m \ln \frac{A}{x}$

T_m= 957 K; A= 10^{13} s^{-1}; R= 0.001987 $kcal^{-1}mol^{-1}$

For the peak maximum at 957 K, crude approximation for desorption activation energy,

$E\alpha = Tm \times 0.066$
$= 957 \times 0.066$
$= 63.162$ kcal mol^{-1}

$X = A \exp\left(\frac{-E}{RT_m}\right)$

$= 10^{13}\ s^{-1} \exp\left(\frac{-63.162 \text{ kcal mol}^{-1}}{0.001987 \text{ kcal}^{-1} \text{ mol}^{-1}. 957K}\right)$
$= 0.3754\ s^{-1}$

E_d = 0.001987 kcal-1mol-1 (957 K) $\ln\left[\frac{10^{13}\ s^{-1}}{0.3754\ s^{-1}}\right]$
$= 63.162$ kcal mol^{-1}

1 cal= 4.184 J

E_d= 264.27 kJ mol^{-1}

Temperature Programmed Reduction (TPR) Calculation

For VPS 6, at T_m= 717 K

Total oxygen reduced= 5.37 $X10^{-4}$ mol g^{-1}

Total oxygen atom reduced =5.37 $X10^{-4}$ mol g^{-1} X 6.02 X 10^{23} atom mol^{-1}
= 3.23 $X10^{20}$ atom g^{-1}

Reduction Activation Energy, $E_r = RT_m \ln \frac{A\,[H_2]}{x \times [H_2]}$

T_m= 717 K; A= 10^{13} s^{-1}; R= 0.001987 $kcal^{-1}mol^{-1}$

$[H_2] = \frac{n}{v} = \frac{0.05}{RT}$

$= \frac{0.05}{(82.056)(298)}$

= 2.0 X 10^{-6} mol cm^{-3}

For the peak maximum at 717 K, crude approximation for reduction activation energy,

Eα= Tm X 0.066
= 717 X 0.066
= 47.322 kcal mol^{-1}

$X = A \exp\left(\frac{-E}{RT_m}\right)$

$= 10^{13}\ s^{-1} \exp\left(\frac{-47.322\ kcal\ mol^{-1}}{0.001987\ kcal^{-1}\ mol^{-1}.\ 717K}\right)$

= 0.3754 s^{-1}

E_r = 0.001987 kcal-1mol-1 (717 K) In $\left[\frac{10^{13}\ s^{-1}\ (2.0 \times 10^{-6}\ mol\ cm^{-3})}{0.3754\ s^{-1}}\right]$

= 28.627 kcal mol^{-1}

1 cal= 4.184 J

E_r= 119.78 kJ mol^{-1}

Appendix G

EDX Calculations

Table: EDX Analysis for Bulk Series

Samples	Phosphorus (P) Atomic weight (%)	Vanadium (V) Atomic weight (%)	P/V Ratio
VPS 6	49.74	50.26	0.990
	18.53	17.41	1.064
	16.52	14.9	1.109
Average			1.054
VPS 18	19.39	18.63	1.041
	18.79	18.15	1.035
	19.98	18.99	1.052
Average			1.043
VPS 30	17.15	18.70	0.917
	20.57	21.05	0.977
	20.28	20.59	0.985
Average			0.960
VPS 75	13.85	13.00	1.065
	15.89	16.11	0.986
	29.75	28.99	1.026
Average			1.026

Table: EDX Analysis for Alkaline-Earth Metals-doped Series

Sample	Phosphorus (P) Atomic weight (%)	Vanadium (V) Atomic weight (%)	P/V Ratio
VPS-Mg	19.59	18.33	1.069
	21.71	20.92	1.038
	24.65	22.64	1.089
Average			1.065
VPS-Ca	19.77	18.48	1.070
	19.52	18.82	1.037
	17.66	15.51	1.139
Average			1.082
VPS-Sr	19.82	18.81	1.054
	21.12	21.03	1.004
	17.95	17.11	1.049
Average			1.036

Table: EDX Analysis for 1 % Ba-doped Series

Sample	Phosphorus (P) Atomic weight (%)	Vanadium (V) Atomic weight (%)	P/V Ratio
VPS Ba-6	20.53	19.54	1.051
	21.96	21.18	1.037
	22.36	21.44	1.043
Average			1.043
VPS Ba-18	22.22	22.16	1.003
	29.58	29.77	0.994
	25.78	24.57	1.049
Average			1.015
VPS Ba-30	20.92	19.73	1.060
	25.73	25.47	1.010
	27.14	26.91	1.009
Average			1.026
VPS Ba-75	24.03	23.92	1.005
	24.88	24.44	1.018
	25.53	26.45	0.965
Average			0.996